

Instrumental variable estimation for compositional treatments

Elisabeth Ailer^{1,2,3,*}, Christian L. Müller^{1,3,4,5}, and Niki Kilbertus^{1,2,3}

¹Helmholtz Munich, Ingolstädter Landstraße 1, Neuherberg, 85764, Germany

²TUM School of Computation, Information and Technology, Technical University of Munich, Boltzmannstraße 3, Garching, 85748, Germany

³Munich Center for Machine Learning (MCML)

⁴Department of Statistics, Ludwig-Maximilian University, Geschwister-Scholl-Platz 1, Munich, 80539, Germany

⁵Center for Computational Mathematics, Flatiron Institute, 162 5th Ave, NY 10010, New York, United States

*Corresponding author: elisabeth.ailer@helmholtz-munich.de

ABSTRACT

Many scientific datasets are compositional in nature. Important biological examples include species abundances in ecology, cell-type compositions derived from single-cell sequencing data, and amplicon abundance data in microbiome research. Here, we provide a causal view on compositional data in an instrumental variable setting where the composition acts as the cause. First, we crisply articulate potential pitfalls for practitioners regarding the interpretation of compositional causes from the viewpoint of interventions and warn against attributing causal meaning to common summary statistics such as diversity indices in microbiome data analysis. We then advocate for and develop multivariate methods using statistical data transformations and regression techniques that take the special structure of the compositional sample space into account while still yielding scientifically interpretable results. In a comparative analysis on synthetic and real microbiome data we show the advantages and limitations of our proposal. We posit that our analysis provides a useful framework and guidance for valid and informative cause-effect estimation in the context of compositional data.

Introduction and Motivation

The statistical modeling of compositional (or relative abundance) data plays a pivotal role in many areas of science, ranging from the analysis of mineral samples or rock compositions in earth sciences [1] to correlated topic modeling in large text corpora [2, 3]. Recent advances in biological high-throughput sequencing techniques, including single-cell RNA-Seq and microbial amplicon sequencing [4, 5], have triggered renewed interest in compositional data analysis. Since only a limited total number of transcripts can be captured in a sample by current sequencing technologies, the resulting count data provides relative abundance information about mRNA transcripts or microbial amplicon sequences, respectively [6, 7].

For example, in microbiome sequencing, this stems from the fact that one cannot easily control for the total number of microbes entering the measurement process. Bacterial microbiome measurements typically come in the form of counts of operational taxonomic units (OTUs) or amplicon sequencing variants (ASVs) derived from high-throughput sequencing of 16S ribosomal RNA (rRNA) [8] and are summarized as taxonomic compositions, e.g., on the species, genus, or family level.

One way of dealing with the available relative abundance information is to normalize read counts by their respective totals, resulting in *compositional data*. Compositional data comprises the proportions of some whole, implying that data points live on the unit simplex $\mathbb{S}^{p-1} := \{x \in \mathbb{R}_{\geq 0}^p \mid \sum_{j=1}^p x_j = 1\}$.

In the microbiome example, assume there are p different microbial taxa that have been identified in a human gut microbiome experiment. A specific gut microbiome measurement is then represented by a vector x , where x_j denotes the relative abundance of taxon j (under an arbitrary ordering of taxa). An increase in x_1 within this composition could correspond to an actual increase in the absolute abundance of the first taxon, while the rest remained constant. However, it could equally result from a decrease of the absolute abundance of the first species with the remaining ones having decreased even more.

Statisticians have recognized the significance of compositional data early on (dating back to Karl Pearson) and tailored models to naturally account for compositionality via simplex arithmetic [1]. Despite these efforts, adjusting predictive statistical and machine learning methods to compositional data remains an active field of research [9, 10, 11, 12, 13, 14, 15, 16, 17, 18].

This work focuses on estimating the causal effect of a composition on a categorical or continuous outcome. Only recently have the fundamental challenges in interpreting causal effects of compositions been acknowledged explicitly [19, 20] with little work on how to estimate such effects from observational data. Our work provides scalable methods that *enable practitioners to answer the simple question: “What is the causal effect of a composition on some outcome of interest?”*

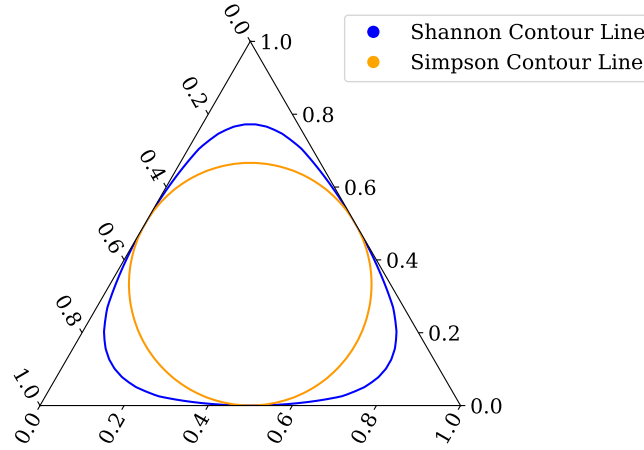


Figure 1. The ternary plot shows an exemplary scenario with $p = 3$. The orange contour contains compositions for which the Simpson diversity is constant, while the blue contour shows compositions for which the Shannon diversity is constant. Shannon diversity changes along contours of Simpson diversity and vice versa.

Pitfalls with Summary Statistics

First, let us motivate the *compositional* aspect of the question. In microbiome research specifically, species diversity became the center of attention to an extent that asking “what is the causal effect of *the diversity* of a composition X on the outcome Y ?” appears more intuitive than asking for the causal effect of individual abundances. In fact, popular books and research articles alike seem to suggest that (bio-)diversity is indeed an important *causal driver* of ecosystem functioning and human health, even though these claims are largely grounded in observational, non-experimental data [21, 22]. Similar summary statistics or low-dimensional representations have been proposed in other domains such as in single-cell RNA data [23]. We now explain why, even in situations where summary statistics appear to be useful proxies, no causal conclusions can be drawn from them.

Let us consider α -diversity as an example of a one-dimensional summary statistic of a microbiome measurement, e.g. $\alpha_{\text{Simpson}} = -\sum_{j=1}^p (x_j)^2$ or $\alpha_{\text{Shannon}} = -\sum_{j=1}^p x_j \log x_j$. The “causal effect” of the diversity α on some outcome of interest Y (e.g., health or disease indicator) is usually considered to be the expected value of Y under an *intervention on the diversity*, i.e., externally setting the diversity to a chosen value α^* , with all host and environmental factors unchanged. This causal effect is commonly denoted by $\mathbb{E}[Y \mid do(\alpha = \alpha^*)]$. When $\mathbb{E}[Y \mid do(\alpha = \alpha_1)] < \mathbb{E}[Y \mid do(\alpha = \alpha_2)]$ for two diversity values α_1, α_2 with $\alpha_1 < \alpha_2$, one would then be tempted to conclude that “increasing diversity α causes an increase in the outcome Y ”, which is often loosely translated to “diversity is a causal driver for health”. We now highlight critical issues with this approach.

(a) When considering the proposed causal effect estimand $\mathbb{E}[Y \mid do(\alpha = \alpha^*)]$ directly, one presupposes the existence of clearly defined interventions on α . However, there are infinitely many ways of changing the diversity of a composition by a fixed amount. This ‘many-to-one’ nature prevents a consistent conceptualization of external interventions. In particular, for a given value of α , there is a $(p - 2)$ -dimensional subspace of \mathbb{S}^{p-1} with that value of α . Hence, an intervention to “increase the diversity of a given composition” by some $\Delta\alpha$ is highly ambiguous. The different ways of achieving this change must be expected to have different implications for the outcome Y . Similarly, most common diversity measures are invariant under permutations of components and the above approach would require us to conclude that all $p!$ permutations of a composition are functionally completely equivalent with regard to the outcome Y —an abstruse claim. *Hence, assigning causal powers to diversity by estimating $\mathbb{E}[Y \mid do(\alpha)]$ is highly ambiguous and does not carry the intended meaning.* This concern is further exacerbated by the difficulty and ambiguity in measuring α -diversity in the first place [7, 24, 25].

(b) The definition of α -diversity is not unique, which could lead to a potential search for positive results by using a different metric [26] or contradictory causal claims. Consider two different one-dimensional summary statistics α_1, α_2 on \mathbb{S}^{p-1} . These can be defined in terms of their contours, i.e., the collection of $(p - 2)$ -dimensional subspaces of \mathbb{S}^{p-1} of constant values of α_1 and α_2 respectively. Since they are different, there will be a contour line of α_1 along which α_2 either increases or decreases. Along this path through compositions, we would have to conclude that the causal effect of one summary statistic is zero, while it is non-zero for the other. See Figure 1 for a visualization. In typical scenarios, there is no “one correct” summary statistic, such that reliable claims even about the sign of the causal effect of a summary statistic of a composition become void.

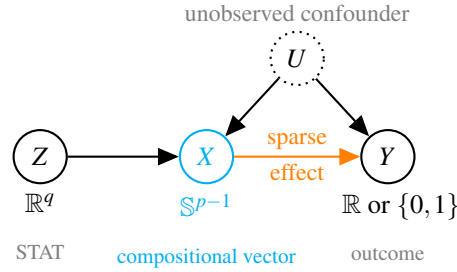


Figure 2. Cause-effect estimation of $X \rightarrow Y$ via an instrumental variable Z for compositional X .

Cause-Effect Estimation with Instrumental Variables

While researchers continue to develop predictive methods for compositional data [16], in most scientific contexts causal effects are of greater interest. For example, the human microbiome co-evolves with its host and the external environment through diet, activity, climate, or geography, etc. leading to plentiful microbiome-host-environment interactions [27]. Carefully designed studies may allow us to control for certain environmental factors and specifics of the host. In fact, several recent works studied the causal mediation effect of the microbiome on health-related outcomes, assuming all relevant covariates are observed and can be controlled for [28, 29, 30, 31, 32, 33, 34], or vice versa, the effect of environmental factors on the microbiome [35]. However, in practice there is little hope of measuring *all* latent factors in these complex interactions. In such a situation, a purely predictive model will suffer from bias due to the unobserved confounders. Such unobserved confounders are a major hurdle in cause-effect estimation broadly and also specifically for compositional causes.

Concretely, without further assumptions, the direct causal effect $X \rightarrow Y$ is not identified from observational data in the presence of unobserved confounding $X \leftarrow U \rightarrow Y$ [36]. One common way to still identify the causal effect from purely observational data is through so-called instrumental variables (IV) [37]. An *instrumental variable* Z is a variable that has an effect on the cause X ($Z \rightarrow X$), but is independent of the confounder ($Z \perp\!\!\!\perp U$), and conditionally independent of the outcome given the cause and the confounder ($Z \perp\!\!\!\perp Y \mid \{X, U\}$). In practice, it can be hard to find valid instruments for a target effect [38], but when they do exist, instrumental variables often render efficient cause-effect estimation possible.

In this work, we develop interpretable methods to estimate the direct causal effect of a *compositional cause* X on a continuous or categorical outcome Y within the IV setting. The question of whether and how cause-effect estimation for compositional treatments under unobserved confounding is possible remains unanswered in the literature, motivating our in-depth analysis of two-stage methods for interpretable cause-effect estimation of individual relative abundances on the outcome. In the analysis, we focus on a careful selection and combination of existing approaches and a thorough examination of potential pitfalls and mis-usage. Our extensive empirical evaluations carefully assess assumptions (additive noise, strong instruments) and model misspecification as a potential obstacle to interpretable and reliable effect estimates. We evaluate the efficacy and robustness of our proposed methods on both synthetic and real data from a mouse experiment, examining how the gut microbiome (X) affects body weight (Y) instrumented by sub-therapeutic antibiotic treatment (STAT) (Z).

The rest of the manuscript proceeds as follows. First, we introduce the concepts of compositional data and instrumental variables in detail. Following this introduction of our methods, we provide some simulation to study the advantage and potential pitfalls in using high-dimensional compositional data in instrumental variable settings. Last but not least, we then apply the methods to a real world dataset.

Methods

Instrumental Variables

We briefly recap the assumptions of the instrumental variable setting as depicted in Figure 2. For an *outcome* (or *effect*) Y , a *treatment* (or *cause*) X , and potential *unobserved confounders* U , we assume access to a discrete or continuous *instrument* $Z \in \mathbb{R}^q$ satisfying (i) $Z \perp\!\!\!\perp U$ (the confounder is independent of the instrument), (ii) $Z \not\perp\!\!\!\perp X$ (“the instrument influences the cause”), and (iii) $Z \perp\!\!\!\perp Y \mid \{X, U\}$ (“the instrument influences the outcome only through the cause”). Our goal is to estimate the direct causal effect of X on Y , written as $\mathbb{E}[Y|do(x)]$ in the do-calculus notation [36] or as $\mathbb{E}[Y(x)]$ in the potential outcome framework [39], where $Y(x)$ denotes the potential outcome for treatment value x . The functional dependencies are $X = g(Z, U)$, $Y = f(X, U)$. While Z, X, Y denote random variables, we also consider a dataset of n i.i.d. samples $\mathcal{D} = \{(z_i, x_i, y_i)\}_{i=1}^n$ from their joint distribution. We arrange observations in matrices or vectors denoted by $\mathbf{X} \in \mathbb{R}^{n \times p}$ or $\mathbf{X} \in (\mathbb{S}^{p-1})^n$, $\mathbf{Z} \in \mathbb{R}^{n \times q}$, $\mathbf{y} \in \mathbb{R}^n$.

Without further restrictions on f and g , the causal effect is not identified [40, 41, 42]. The most common assumption leading to identification is that of *additive noise*, namely $Y = f(X) + U$ with $\mathbb{E}[U] = 0$ but not necessarily $X \perp\!\!\!\perp U$. Here, we

overload the symbols f and g for simplicity. The implied Fredholm integral equation of first kind $\mathbb{E}[Y | Z] = \int f(x) dP(X | Z)$ is generally ill-posed. While the linear case is well understood [37], under certain regularity conditions the IV problem can be solved consistently even for non-linear f , see e.g., [43, 44] and more recently [45, 46, 47, 48]. However, in this case the problem is typically under-specified in that multiple f are compatible with the observed data and regularization techniques are typically used to obtain a unique solution—typically the smallest compatible f according to some norm. It is thus difficult to interpret estimates of non-linear causal-effects in a way that aids understanding of the underlying processes.

In the simplest case, where $X \in \mathbb{R}^p$ and f, g are linear, a standard *instrumental variable estimator* is

$$\hat{\beta}_{iv} = (\mathbf{X}^T \mathbf{P}_Z \mathbf{X})^{-1} \mathbf{X}^T \mathbf{P}_Z \mathbf{y} \quad (1)$$

with $\mathbf{P}_Z = \mathbf{Z}(\mathbf{Z}^T \mathbf{Z})^{-1} \mathbf{Z}^T$ [37]. For the *just-identified* case $q = p$ as well as the over-identified case $q > p$, this estimator is consistent and asymptotically unbiased, albeit not unbiased. In the *under-identified* case $q < p$, where there are fewer instruments than treatments, the orthogonality of Z and U does not imply a unique solution. Again, regularization or other objectives such as sparsity assumptions have been proposed to obtain a unique solution within the space of compatible β [49, 50, 51]. The estimator $\hat{\beta}_{iv}$ can also be interpreted as the outcome of a *two-stage least squares* (2SLS) procedure consisting of (1) regressing \mathbf{X} on \mathbf{Z} via OLS $\hat{\delta} = (\mathbf{Z}^T \mathbf{Z})^{-1} \mathbf{Z}^T \mathbf{X}$, and (2) regressing \mathbf{y} on the predicted values $\hat{\mathbf{X}} = \mathbf{Z} \hat{\delta}$ via OLS, again resulting in $\hat{\beta}_{iv}$. Practitioners are typically discouraged from using the manual two-stage approach, because the OLS standard errors of the second stage are wrong—a correction is needed [37]. However, we note that the point estimator obtained by the manual two-stage procedure is equivalent to Equation (1).

Moreover, the two-stage description suggests that the two-stages are independent problems and thereby seems to invite us to mix and match different regression methods as we see fit. The authors in [37] highlight that the asymptotic properties of $\hat{\beta}_{iv}$ rely on the fact that for OLS the residuals of the first stage are uncorrelated with the instruments \mathbf{Z} . Hence, for OLS we achieve consistency of $\hat{\beta}_{iv}$ *even when the first stage is misspecified*. For a non-linear first stage regression we may only hope to achieve uncorrelated residuals asymptotically when the model is correctly specified. Replacing the OLS first stage with a non-linear model is known as the “forbidden regression”, a term commonly attributed to Prof. Jerry Hausmann. Angrist and Pischke acknowledge that the practical relevance of the forbidden regression is not well understood. When also the second stage is assumed to be non-linear, one would require independence of the first stage residuals from Z . Starting with [52] there is now a rich literature on the circumstances under which “manual 2SLS” with non-linear first (and/or second) stage can yield consistent causal estimators. Primarily interested in *compositional* treatments X , we cannot directly use OLS for either stage. Since there is no theoretical guidance for this case, we assess our options empirically, paying great attention to potential issues due to the “forbidden regression” and misspecification in our proposed methods.

Compositional Data

Simplex geometry

The authors in [1] introduced the *perturbation* and *power transformation* as the simplex \mathbb{S}^{p-1} counterparts to addition and scalar multiplication of Euclidean vectors in \mathbb{R}^p :

<p>Perturbation</p> $\oplus : \mathbb{S}^{p-1} \times \mathbb{S}^{p-1} \rightarrow \mathbb{S}^{p-1}$ $x \oplus w = C(x_1 w_1, \dots, x_p w_p)$		<p>Power transformation</p> $\odot : \mathbb{R} \times \mathbb{S}^{p-1} \rightarrow \mathbb{S}^{p-1}$ $a \odot x := C(x_1^a, x_2^a, \dots, x_p^a)$
--	--	--

Here, the *closure operator* $C : \mathbb{R}_{\geq 0}^p \rightarrow \mathbb{S}^{p-1}$ normalizes a p -dimensional, non-negative vector to the simplex $C(x) := x / \sum_{i=1}^p x_i$. Together with the dot-product

$$\langle x, w \rangle := \frac{1}{2p} \sum_{i,j=1}^p \log\left(\frac{x_i}{x_j}\right) \log\left(\frac{w_i}{w_j}\right) \quad (2)$$

the tuple $(\mathbb{S}^{p-1}, \oplus, \odot, \langle \cdot, \cdot \rangle)$ forms a finite-dimensional real Hilbert space [53] allowing to transfer usual geometric notions such as lines and circles from Euclidean space to the simplex.

Coordinate representations

The p entries of a composition remain dependent via the unit sum constraint, leading to \mathbb{S}^{p-1} having dimension $p - 1$. To deal with this fact, different invertible log-based transformations have been proposed, for example the additive log ratio, centered log ratio [1], and isometric log ratio [54] transformations

$$\text{alr}(x) = V_a \log(x) \in \mathbb{R}^{p-1}, \quad \text{clr}(x) = V_c \log(x) \in \mathbb{R}^p, \quad \text{ilr}(x) = V_l \log(x) \in \mathbb{R}^{p-1}, \quad (3)$$

where the logarithm is applied element-wise and the matrices $V_a, V_l \in \mathbb{R}^{(p-1) \times p}$ and $V_c \in \mathbb{R}^{p \times p}$ are defined in Supplementary Material S2. While ilr is a vector space isomorphism that preserves a one-to-one correspondence between all components except for one, which is chosen as a fixed reference point to reduce the dimensionality (we choose x_p , but any other component works), it is not an isometry, i.e., it does not preserve distances or scalar products. Both clr and ilr are also isometries, but clr only maps onto a subspace of \mathbb{R}^p , which often renders measure theoretic objects such as distributions degenerate. As an isometry between \mathbb{S}^{p-1} and \mathbb{R}^{p-1} , ilr allows for an orthonormal coordinate representation of compositions. However, it is hard to assign meaning to the individual components of $\text{ilr}(x)$, which all entangle a different subset of relative abundances in x leading to challenges for interpretability [55]. Therefore, alr remains a useful tool in statistical analyses where interpretability is required despite the lack of the isometric property.

Log-contrast estimation

The key advantage of such coordinate transformations is that they allow us to use regular multivariate data analysis methods (typically tailored to Euclidean space) for compositional data. For example, we can directly fit a linear model $y = \beta_0 + \beta^T \text{ilr}(x) + \varepsilon$ on the ilr coordinates via ordinary least squares (OLS) regression. However, in real-world datasets, p is often a large number capturing “all possible components in a measurement”, leading to $p \gg n$ with each of the n measurements being sparse, i.e., a substantial fraction of x being zero. Moreover, in many (especially high-dimensional) situations only few components exert direct causal influence on the outcome. Both overparameterization $p \gg n$ as well as assuming sparse effects call for regularization. The problem with enforcing sparsity in a “linear-in- ilr ” model is that a zero entry in β does not correspond directly to a zero effect of the relative abundance of any single component. This motivates *log-contrast* estimation [56] with a sparsity penalty [57, 58, 59]

$$\min_{\beta} \sum_{i=1}^n \mathcal{L}(x_i, y_i, \beta) + \lambda \|\beta\|_1 \quad \text{s.t.} \quad \sum_{i=1}^p \beta_i = 0. \quad (4)$$

In our examples, we focus mostly on continuous $y \in \mathbb{R}$ and the squared loss $\mathcal{L}(x, y, \beta) = (y - \beta^T \log(x))^2$. However, our framework also supports the Huber loss for robust log-contrast regression as well as an optional joint concomitant scale estimation for both losses [59, 60]. Moreover, for classification tasks with $y \in \{0, 1\}$, we can directly use the squared Hinge loss (or a “Huberized” version thereof) for \mathcal{L} , see Supplementary Material S7 for details. These flexible estimation formulations respect the compositional nature of x while retaining the association between the entry β_i and the relative abundance of the individual component x_i . Even though, due to the additional sum constraint, individual components of β are still not—and can never be—entirely disentangled.

Logs and zeros

In the previous paragraphs, we introduced multiple log-based coordinate representations for compositions and at the same time claimed that measurements are often sparse in relevant settings. Since the logarithm is undefined for zero entries, a simple strategy is to add a small constant to all absolute counts, so called *pseudo-counts* [61, 62]. These pseudo-counts are particularly popular in the microbiome and single-cell RNA literature where there are many more possible taxa/genes (up to tens of thousands) that occur in any given sample. Despite the simplicity of adding a constant pseudo-count, for example 0.5, recent work gives theoretical and empirical evidence for this approach [63], which we also use here.

Summary statistics

Traditionally, interpretability issues around compositions have been circumvented by focusing on summary statistics instead of individual relative abundances. One of the key measures to describe ecological populations is *diversity*. Diversity captures the variation within a composition and is in this context often called α -diversity. There is no unique definition of α -diversity. Among the most common ones in the literature are *richness*, i.e. the number of non-zero entries denoted as $\|x\|_0$, *Shannon diversity* $-\sum_{j=1}^p x_j \log(x_j)$ and *Simpson diversity* $-\sum_{j=1}^p x_j^2$. Especially in the microbial context, there exist entire families of diversity measures taking into account species, functional, or phylogenetic similarities between taxa and tracing out continuous parametric profiles for varying sensitivity to highly-abundant taxa. See for example [64, 65, 66] for an overview of the possibilities and choices of estimating α -diversity in a specific application. While the popularity of α -diversity for assessing the impact and health of microbial compositions [67] seemingly renders it a natural choice for causal queries, we argue that such claims are misleading and void of a solid foundation.

Methods for Higher Dimensional Causes

In this section we develop methods to reason about the effects of hypothetical interventions on the relative abundance of individual components from observational data.

- *2SLS*: As the first baseline, we run 2SLS from Equation (1) directly on $X \in \mathbb{S}^{p-1}$ ignoring its compositional nature.

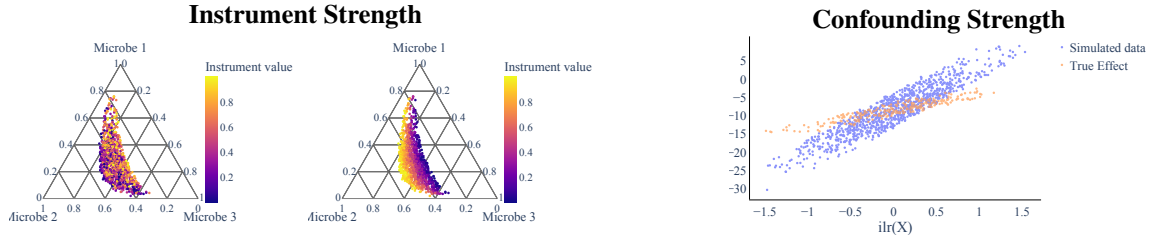


Figure 3. Visualization of a Setting A ($p = 3, q = 2$): The left panel shows both a weak (left) and a strong (right) instrument. The right panel shows a discrepancy between the true causal effect and the observed effect which stems from a confounding factor.

- *Only LC* For completeness, as the second baseline, we run log-contrast (LC) estimation for the second stage only, thereby entirely ignoring confounding.
- $2SLS_{ILR}$: 2SLS with $\text{ilr}(X) \in \mathbb{R}^{p-1}$ as the treatment; since OLS minima do not depend on the chosen basis, parameter estimates for different log-transformations of X are related via fixed linear transformations. Hence, as long as no sparsity penalty is added, ilr and alr regression yield equivalent results. The isometric ilr coordinates are useful due to the consistency guarantees of 2SLS given that $\mathbf{Z}^T \text{ilr}(\mathbf{X})$ has full rank. For interpretability, alr coordinates can be beneficial as individual coordinates correspond to individual components (given a reference). The respective coordinate transformations are given in Supplementary Material S2.
- KIV_{ILR} : Following [45] we replace OLS in $2SLS_{ILR}$ with kernel ridge regression in both stages to allow for non-linearities. Like $2SLS_{ILR}$, KIV_{ILR} cannot enforce sparsity in an interpretable fashion.
- $ILR+LC$: To account for sparsity, we use sparse log-contrast estimation (see Equation (4)) for the second stage, while retaining OLS to ilr coordinates for the first stage. Log-contrast estimation conserves interpretability in that the estimated parameters correspond directly to the effects of individual relative abundances.
- $DIR+LC$: Finally, we circumvent log-transformations entirely and deploy regression methods that naturally work on compositional data in both stages. For the first stage, we use a Dirichlet distribution—a common choice for modeling compositional data—where $X | Z \sim \text{Dirichlet}(\alpha_1(Z), \dots, \alpha_p(Z))$ with density $B(\alpha_1, \dots, \alpha_p)^{-1} \prod_{j=1}^p x_j^{\alpha_j - 1}$ where we drop the dependence of $\alpha = (\alpha_1, \dots, \alpha_p) \in \mathbb{R}^p$ on Z for simplicity. With the mean of the Dirichlet distribution given by $\alpha / \sum_{j=1}^p \alpha_j$, we account for the Z -dependence via $\log(\alpha_j(Z_i)) = \omega_{0,j} + \omega_j^T Z_j$. We then estimate the newly introduced parameters $\omega_{0,j} \in \mathbb{R}$ and $\omega_j \in \mathbb{R}^q$ via maximum likelihood estimation with ℓ_1 regularization. For the second stage we again resort to sparse log-contrast estimation. If the non-linear first stage is misspecified, the “forbidden regression” bias may distort effect estimates of this approach. This is contrasted by Dirichlet regression potentially resulting in a better fit of the data than linearly modeling log-transformations.

We highlight that only $ILR+LC$ and $DIR+LC$ accommodate all relevant requirements: (i) unobserved confounding, (ii) compositional treatments, (iii) sparse effects, and (iv) interpretable estimates.

Simulation Studies

Data Generation

For the evaluation of our methods we require the ground truth causal effect to be known. Since unobserved confounders (and thus counterfactuals) are never observed in practice (by definition), this can only be achieved via synthetic data. We simulate data (in two different settings) to maintain control over ground truth effects, confounding strength, potential misspecification, and the strength of instruments (see Fig. 3).

- *Setting A*: The first setting is

$$\begin{aligned} Z_j &\sim \text{Unif}(0, 1), & U &\sim \mathcal{N}(\mu_c, 1), \\ \text{ilr}(X) &= \alpha_0 + \alpha^T Z + U c_X, & Y &= \beta_0 + \beta^T \text{ilr}(X) + U c_Y, \end{aligned} \quad (5)$$

where we model $\text{ilr}(X) \in \mathbb{R}^{p-1}$ directly and $\mu_c, c_Y \in \mathbb{R}$, $\alpha_0, c_X \in \mathbb{R}^{p-1}$, $\alpha \in \mathbb{R}^{q \times (p-1)}$ are fixed up front. Our goal is to estimate the causal parameters $\beta \in \mathbb{R}^{p-1}$ and the intercept $\beta_0 \in \mathbb{R}$. This setting satisfies the standard 2SLS assumptions

(linear, additive noise) and all our linear methods are thus *wellspecified*. To explore effects of *misspecification*, we also consider the same setting only replacing (using $\mathbf{1} = (1, \dots, 1)$)

$$Y = \beta_0 + \frac{1}{100} \mathbf{1}^T (\text{ilr}(X) + 1)^2 + 10 \cdot \mathbf{1}^T \sin(\text{ilr}(X)) + c_Y U. \quad (6)$$

- *Setting B*: We consider a sparse effect model for $X \in \mathbb{S}^{p-1}$ which is more realistic for higher-dimensional compositions. Note that some parameter dimensions are different, i.e., the same symbols have different meanings in the settings A and B. With $\mu = \alpha_0 + \alpha^T Z$ for fixed $\alpha_0 \in \mathbb{R}^p$, $\alpha \in \mathbb{R}^{q \times p}$ we use

$$\begin{aligned} Z_j &\sim \text{Unif}(Z_{\min}, Z_{\max}), & U &\sim \text{Unif}(U_{\min}, U_{\max}), \\ X &\sim \mathcal{C}(\text{ZINB}(\mu, \Sigma, \theta, \eta)) \oplus (U \odot \Omega_C), \\ Y &= \beta_0 + \beta^T \log(X) + c_Y^T \log(U \odot \Omega_C). \end{aligned} \quad (7)$$

The treatment X is assumed to follow a zero-inflated negative binomial (ZINB) distribution [68], commonly used for modelling count data with excess zeros [69]. Here, $\eta \in (0, 1)$ is the probability of zero entries, $\Sigma \in \mathbb{R}^{p \times p}$ is the covariance matrix, and $\theta \in \mathbb{R}$ the shape parameter. The confounder $U \in [U_{\min}, U_{\max}]$ perturbs this base composition in the direction of another fixed composition $\Omega_C \in \mathbb{S}^{p-1}$ scaled by U . In simplex geometry $x_0 \oplus (U \odot x_1)$ corresponds to a line starting at x_0 and moving along x_1 by a fraction U . A linear combination of the log-transformed perturbation enters Y additively with weights $c_Y \in \mathbb{R}^p$ controlling confounding strength. All other parameter choices are given in Supplementary Material S6. This setting is linear in how Z enters μ and how U enters X and Y in the simplex geometry. All our two-stage models are (intentionally) misspecified in the first stage for setting B.

The precise choices of all parameters for the different empirical evaluations are described in the appendix (Supplementary Material S6). All relevant code is available at <https://github.com/EAiler/causal-compositions>.

Metrics and Evaluation

Appropriate evaluation metrics are key for cause-effect estimation tasks. We aim at capturing the average causal effect (under interventions) and the causal parameters when warranted by modeling assumptions. When the true effect is linear in $\log(X)$, we can compare the estimated causal parameters $\hat{\beta}$ from 2SLS_{ILR}, ILR+LC, and DIR+LC with the ground truth β directly. In these linear settings, we report causal effects of individual relative abundances X_j on the outcome Y via the mean squared difference (β -MSE) between the true and estimated parameters β and $\hat{\beta}$. Moreover, we also report the number of falsely predicted non-zero entries (FNZ) and falsely predicted zero entries (FZ), which are most informative in sparse settings and metrics of key interest to biostatisticians.

In the general case, where a measure for identification of the interventional distribution $P(Y | do(X))$ is not straightforward to evaluate, we focus on the *out of sample error* (OOS MSE): For the true causal effect we first draw an i.i.d. sample $\{x_i\}_{i=1}^m$ from the data generating distribution (that are not in the training set, i.e., out of sample) and compute $\mathbb{E}_U[f(x_i, U)]$ for the known $f(X, U)$, the expected Y under intervention $do(x_i)$. We use $m = 250$ for all experiments. OOS MSE is then the mean square difference to our second-stage predictions $\hat{f}(x_i)$ on these out of sample x_i . Because in real observational data we do not have access to $P(Y | do(X))$ (but only the conditional distribution $P(Y | X)$), we can not evaluate OOS MSE in real-world observational data.

We run each method for 50 random seeds in setting A (Equation (5)), and 20 random seeds in setting B (Equation (7)). In result tables, we report mean and standard error over these runs. The sample size is $n = 1000$ in the low-dimensional case ($p = 3$) and $n = 10,000$ in the higher-dimensional cases ($p = 30$, $p = 250$). Additionally, we report results for an overparameterized setting with $n = 100$ and $p = 250$. Supplementary Materials S6 and S8 contain further explanations and more detailed results. Note, that since alr coordinates for X yield equivalent optimization minima as ILR+LC, we only report results from ILR+LC. All numbers match precisely for ALR+LC in our empirical evaluation.

Results for Low-Dimensional Compositions

We first consider settings A and B with $p = 3$ and $q = 2$. The top section of Tables 1 and 2 shows our metrics for all methods. First, effect estimates are far off when ignoring the compositional nature (2SLS) or the confounding (Only LC) as expected. Also, recent non-linear IV methods such as [47, 70, 71] could not overcome the issues of 2SLS in this setting. Without sparsity in the second stage, 2SLS_{ILR} and ILR+LC yield equivalent estimates in this low-dimensional linear setting—we only report ILR+LC. ILR+LC (and equivalent methods) succeed in cause-effect estimation under unobserved confounding: they recover the true causal parameters with high precision on average (low β -MSE) and thus achieve low OOS MSE. While DIR+LC performs reasonably well in setting A, setting B surfaces that despite being a seemingly plausible approach with powerful regression techniques, DIR+LC suffers substantially under a misspecified first-stage.

		Setting A, Equation (5)			
Dim.	Method	OOS MSE	β -MSE	FZ	FNZ
$p = 3$ $q = 2$	DIR+LC	0.58 \pm 0.08	1.6 \pm 0.17	0.0	0.0
	ILR+LC [†]	0.37 \pm 0.07	1.1 \pm 0.15	0.0	0.0
	KIV _{ILR}	0.37 \pm 0.07	—	—	—
	Only LC	15.03 \pm 0.20	32.6 \pm 0.14	0.0	0.0
	2SLS	> 200	> 5k	0.0	0.0
$p = 30$ $q = 10$	ILR+LC	0.42 \pm 0.08	0.22 \pm 0.01	0.0	12.0
	KIV _{ILR}	240.6 \pm 35.7	—	—	—
	Only LC	24.4 \pm 0.37	1.9 \pm 0.00	0.0	12.3
$p = 250$ $q = 10$	ILR+LC	0.67 \pm 0.14	0.22 \pm 0.02	0.0	0.0
	KIV _{ILR}	5060.5 \pm 1196.2	—	—	—
	Only LC	30.8 \pm 0.48	143.3 \pm 0.27	3.0	1.0

[†] Identical to 2SLS_{ILR} in low-dimensional setting without sparsity.

Table 1. Results for setting A (fully linear in $\text{ilr}(X)$).

		Setting B, Equation (7)			
Dim.	Method	OOS MSE	β -MSE	FZ	FNZ
$p = 3$ $q = 2$	DIR+LC	> 10k	> 2k	0.0	0.0
	ILR+LC [†]	20.3 \pm 4.85	9.9 \pm 3.3	0.0	0.0
	KIV _{ILR}	19.2 \pm 4.42	—	—	—
	Only LC	269.0 \pm 6.85	129.8 \pm 2.13	0.0	0.0
	2SLS	> 15k	> 300k	0.0	0.0
$p = 30$ $q = 10$	ILR+LC	120.4 \pm 25.1	37.0 \pm 15.1	0.0	13.3
	KIV _{ILR}	287.2 \pm 19.1	—	—	—
	Only LC	3863.8 \pm 166.3	458.8 \pm 12.2	3.4	15.8
$p = 250$ $q = 10$	ILR+LC	99.1 \pm 7.9	24.4 \pm 4.30	0.13	0.39
	KIV _{ILR}	622.8 \pm 30.1	—	—	—
	Only LC	3366.0 \pm 166.3	498.3 \pm 17.2	6.9	1.9

[†] Identical to 2SLS_{ILR} in low-dimensional setting without sparsity.

Table 2. Results for setting B (first stage ZINB with sparse effects in higher dimensions), where all our two-stage methods are (intentionally) misspecified in the first stage.

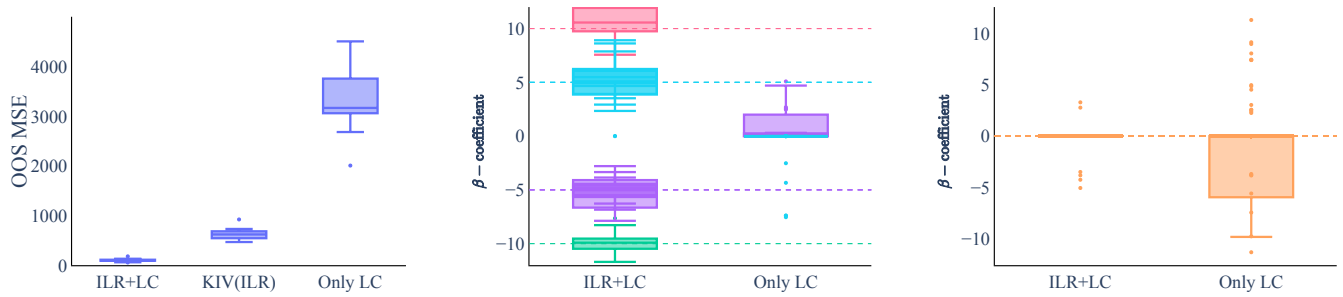


Figure 4. Boxplots of the results for setting B in Table 2 with $p = 250, q = 10$. We show OOS MSE (left), recovery of non-zero β coefficients (middle), and recovery of zero β coefficients.

Results for High-Dimensional Compositions

We now consider the challenging cases $p = 30$ and $p = 250$ with $q = 10$ and sparse ground truth β for settings A and B (8 non-zeros: 3 times -5 and 5 and once -10 and 10) in the bottom sections of Tables 1 and 2. ILR+LC deals well with sparsity: unlike Only LC, it identifies non-zero parameters perfectly ($FZ = 0$) and rarely predicts false non-zeros. It also identifies the true β and accordingly predicts interventional effects (OOS MSE) well. DIR+LC and 2SLS_{ILR} fail entirely in these settings because the optimization does not converge. While we could get KIV_{ILR} to return a solution, tuning the kernel hyperparameters for high-dimensional ilr coordinates becomes increasingly challenging, which is reflected in poor OOS MSE. In Figure 4 we show detailed results for the most challenging setting (setting B with $p = 250$ and $q = 10$) including the OOS MSE (left), recovery of individual non-zero coefficients (middle), and recovery of zero coefficients (right). Analogous plots for all other settings can be found in Supplementary Material S8.

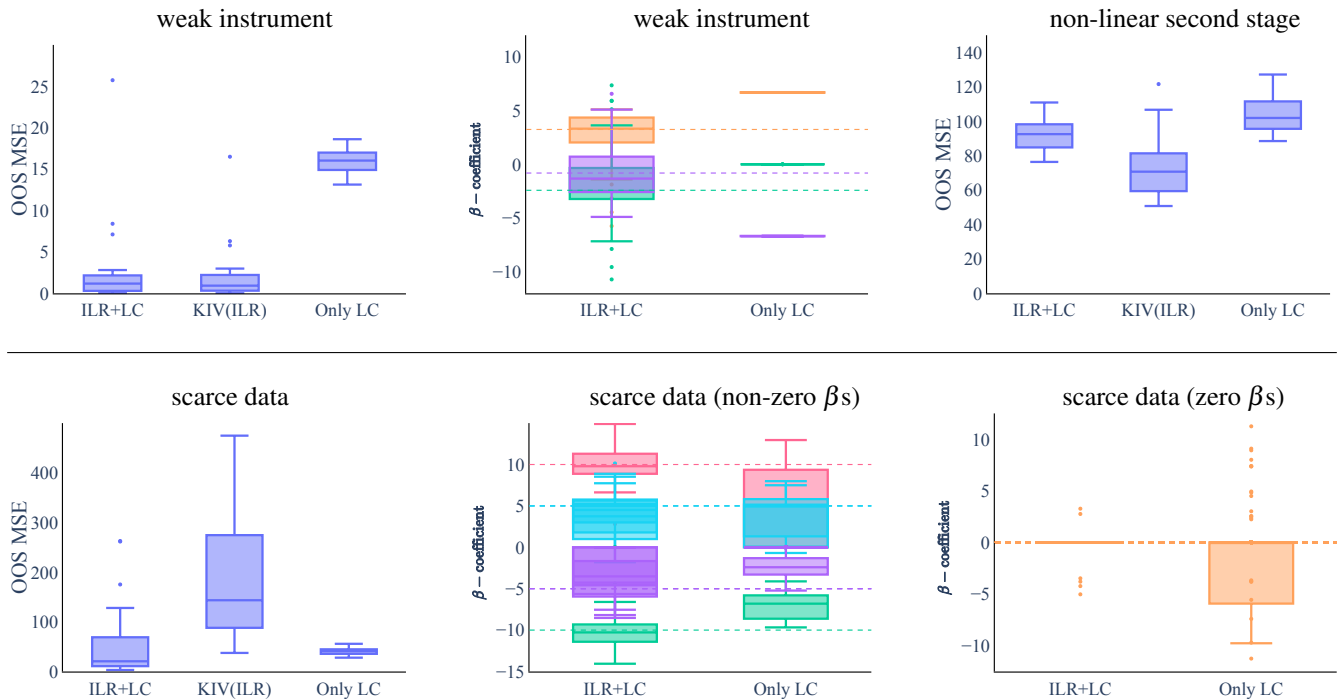


Figure 5. We display OOS MSE and β -MSE (for non-zero coefficients and where applicable) for our robustness checks. All results and further visualizations are in Supplementary Material S8.

Robustness Checks

Due to the inherent entanglement via the unit sum constraint, analyses involving compositional data are generically hard to interpret. Causal analyses involving compositions in the instrumental variable setting are further challenged by potential violations of assumptions such as weak instruments or misspecification. We assess the sensitivity of our proposed methodology to such potential pitfalls in the following scenarios.

Weak Instruments

“Strong instruments” are a prerequisite for successful two-stage estimation in the instrumental variable setting and one of the key discussion points in real-world applications of IV. Nevertheless, how to measure instrument validity is not unambiguously clarified, relying on heuristics and empirically derived best practices. In the linear setting, instrument strength for $p = 1$ can be approximated via a first-stage F-statistic with a value greater than 10 generally being considered sufficient to avoid weak instrument bias in 2SLS [72]. For $p > 1$, measuring instrument strength is more challenging even in the linear case [73]. Therefore, we report first-stage F-statistics for each dimension of X as a proxy for instrument strength.

When instruments are weak, the estimation bias can theoretically become arbitrarily large (even in the limit of infinite data). To assess the sensitivity of our methods to weak instrument bias, we re-analyze setting A ($p = 3$ and $q = 2$) only changing the dependence of X and Z to be weak with first-stage F-statistic values of 6.9 and 4.7 for the two components of $\text{ilr}(X)$. In the linear setting, we can directly control instrument strength via α (see Equation (5)).

The first row in Table 3 summarizes our results for weak instruments: the two-stage methods have a substantially higher variation in their estimates, both for OOS MSE and $\hat{\beta}$ compared to the strong instrument setting in Tables 1 and 2. As the second stage has not changed, Only LC performs equally bad. Notably, while the wellspecified two-stage methods ILR+LC and 2SLS_{ILR} seem to do worse than Only LC, the large OOS MSE and β -MSE are mostly due to outliers. Figure 5 shows that the range of β estimates still cover the true values for ILR+LC and 2SLS_{ILR}, while Only LC is systematically off with low variance (confidently wrong). DIR+LC now not only suffers from the misspecified first stage but also the weak instrument resulting in virtually useless estimates. The surprisingly good performance of KIV_{ILR} in this specific setting is unexpected and cannot be consistently reproduced over different weak instrument scenarios: the performance is highly volatile and often worse than ILR+LC. Therefore, despite the good performance for these specific parameters, we find that more flexible methods are also affected heavily by weak instruments. In general, while two-stage estimates generally cannot be broadly trusted when instruments are weak, reverting to Only LC is potentially even more detrimental because the estimated coefficients are systematically off.

Non-linear Second Stage

Well-specification is typically impossible to ascertain in practice and most real-world examples are likely not perfectly linear even when the linearity assumption can be defended. Therefore, we introduce a non-linear f for setting A with $p = 3$ and $q = 2$ (Equation (6)), resulting in a misspecified second stage for all our methods except KIV_{ILR}, which can in principle capture non-linearities. Note that β cannot be interpreted directly as causal parameters when the true causal effect depends non-linearly on $\text{ilr}(X)$. The results in the second row of Table 3 show that DIR+LC (doubly misspecified) and 2SLS (ignoring compositionality) again fail. Moreover, in this non-linear scenario KIV_{ILR} beats ILR+LC (both still outperforming Only LC) and we expect the difference to grow as the non-linearity of f increases.

Scarce Data

Finally, we return to the original setting A ($p = 250$, $q = 10$, linear in both stages), but mimic a scarce data scenario with $n = 100$. The third row in Table 3 clearly highlights again how the lack of regularization becomes problematic for 2SLS_{ILR} and KIV_{ILR}. Compared to the larger dataset, also our regularized two-stage methods naturally exhibit higher variation in their estimates. Notably, Only LC appears to compare favorably to ILR+LC in OOS MSE, but β -MSE surfaces its failure to accurately recover causal parameters. We thus conclude that despite increased variability, the ILR+LC is still better equipped to recover β in the small data regime (see Figure 5).

Case study on murine sub-therapeutic antibiotic treatment

We consider the mouse dataset described by [74] and analyzed in [30] using causal mediation. A total of 57 newborn mice were assigned randomly to a sub-therapeutic antibiotic treatment (STAT) during their early stages of development. Sub-therapeutic antibiotic treatment means that the administered doses of antibiotics are too small to be detectable in the mice’ bloodstream. There were 35 mice in the treatment group and 22 mice in the control group. After 21 days, the gut microbiome composition of each mouse was recorded. We are interested in the causal effect of the gut microbiome composition on body weight $Y \in \mathbb{R}$ of the mice (at sacrifice).

We assume a valid instrument due to the following characteristics in the data generation: The random assignment of the antibiotic treatment ensures independence of potential confounders such as genetic factors ($Z \perp\!\!\!\perp U$). The sub-therapeutic dose implies that antibiotics can not be detected in the mice’ blood, providing reason to assume no effect of the antibiotics on the weight other than through its effect on the gut microbiome ($Z \perp\!\!\!\perp Y \mid \{U, X\}$).

Finally, we observe empirically, that there are statistically significant differences of microbiome compositions between the treatment and control groups ($Z \not\perp\!\!\!\perp X$) based on the first stage F-statistic. Thus, the sub-therapeutic antibiotic treatment is a good candidate for an instrument $Z \in \{0, 1\}$ in estimating the effect $X \rightarrow Y$. Note, however, that this work is focused

Scenario	Method	OOS MSE	β -MSE
Weak Instruments	DIR+LC	7.1 \pm 2.6	43.2 \pm 10.3
	ILR+LC [†]	3.6 \pm 1.3	26.0 \pm 5.6
	KIV _{ILR}	2.7 \pm 0.9	—
	Only LC	15.9 \pm 0.20	52.2 \pm 0.18
	2SLS	> 100	> 5k
Non-Linearity	DIR+LC	135.6 \pm 6.34	—
	ILR+LC [†]	92.0 \pm 1.2	—
	KIV _{ILR}	73.4 \pm 2.28	—
	Only LC	104.1 \pm 1.43	—
	2SLS	> 300	—
Scarce Data	ILR+LC	45.1 \pm 7.90	72.8 \pm 8.3
	KIV _{ILR}	290.8 \pm 62.5	—
	Only LC	40.5 \pm 1.00	196.4 \pm 8.7
	2SLS _{ILR}	> 10k	> 2 · 10 ²⁴

[†] Identical to 2SLS_{ILR} in low-dimensional setting without sparsity.

Table 3. Results for various robustness checks.

on methods rather than novel biological insights as more scrutiny of the IV assumptions would be required for substantive biological claims.

Figure 6 highlights the two most influential microbes on the genus level for our two-stage ILR+LC estimator and to the non-causal baseline Only LC, respectively. In the causal setting, we estimate the log-ratio of Blautia to Anaerostipes to be most influential for weight gain whereas standard log-contrast regression deems the ratio of an unclassified Enterobacteria genus to Lactobacillus to be the most predictive genus pair. This discrepancy suggests that the second stage might be subject to confounding. However, the mediation analysis on the same dataset in [30] posits a negative mediation effect of Lactobacillus on weight gain, consistent with the non-causal baseline model. This highlights the fact that different causal models provide alternative interpretation of the data that can only resolved by follow-up biological experiments.

Finally, we also assessed the influence of taxonomic aggregation levels and different loss functions on the results (see Supplementary Material S5). We observed that our causal model is robust to the choice of the loss function in terms of selected taxa whereas the baseline model found loss-function dependent sets of predictive taxa (see Supplementary Material Figure S2).

Discussion

In this work, we developed and analyzed methods for cause-effect estimation with compositional causes under unobserved confounding in instrumental variable settings. First, we succinctly expose that the common portrayal of summary statistics as a decisive (rather than merely descriptive) description of compositions is misguided. Instead, we advocate for causal effects to be estimated from the entire composition vector directly to establish meaningful and interpretable causal links. As a result, analysts cannot tap into a collection of well established cause-effect estimation tools for scalar data, but are instead faced with a large number of possible components (calling for sparsity-enforcing methods) and typically have to deal with unobserved confounding. Given the potentially profound impact of microbiome or single cell RNA data on advancing human health or of species abundances on global health, it is of vital importance that we face these challenges and develop interpretable methods to obtain causal insights from compositional data.

To this end, we carefully developed and assessed the effectiveness of various methods to not only reliably recover causal effects (OOS MSE), but also yield *interpretable and sparse* effect estimates for individual abundances (β -MSE, FZ, FNZ) whenever applicable. We also put special emphasis on how IV assumptions (misspecification, weak instrument bias) interact with compositionality. Our extensive empirical results for different two-stage methods highlight that accounting for the compositional nature as well as confounding is not optional. The overall failure of DIR+LC shows that not any seemingly suitable compositional technique can be trusted to yield reliable estimates in a manual two-stage procedure—careful analysis is needed. We have identified ILR+LC, to work reliably in wellspecified sparse and non-sparse settings as well as being relatively robust to first- and (small) second-stage misspecifications (i.e., non-linearities) and scarce data. It also yields interpretable estimates for individual components. When interpretability is not required or second-stage non-linearities are strong, KIV_{ILR} can still perform well under these relaxed assumptions albeit being challenging to tune for large p and unable to incorporate sparsity. As expected, valid instruments are required for all our two-stage methods. Taken together, our results on the efficacy

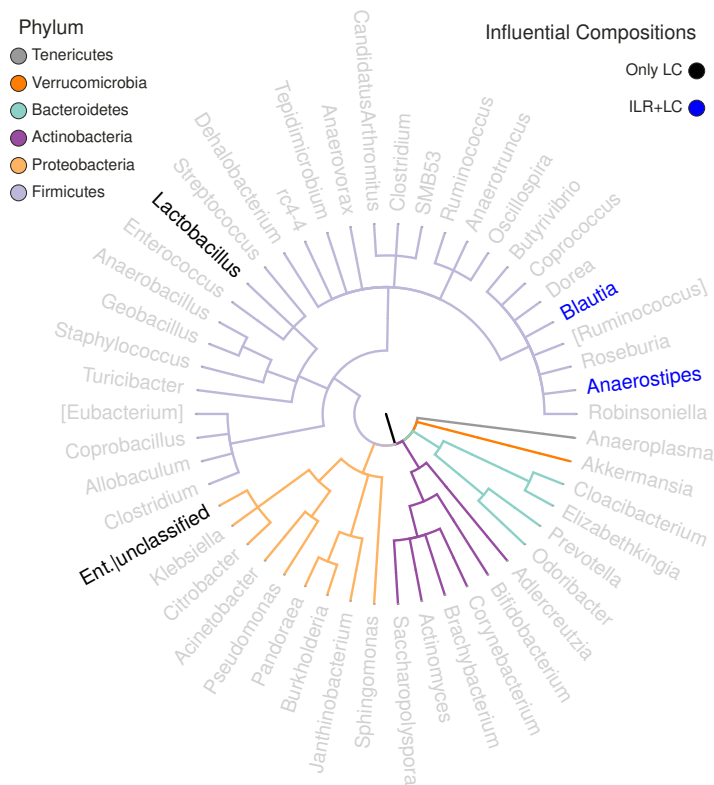


Figure 6. Taxonomic tree of the microbiome data at genus level. The influential log-ratios for both Only Second LC and ILR+LC are highlighted in black and blue, respectively.

and robustness of our methods in simulation and on real microbiome data provide first recommendations for practitioners to fully integrate compositional data into cause-effect estimation.

Acknowledgments

We thank Dr. Chan Wang and Dr. Huilin Li, NYU Langone Medical Center, for kindly providing the pre-processed murine amplicon and associated phenotype data used in this study. We thank Léo Simpson, TU München, and Alice Sommer, LMU München, for kindly and patiently providing their technical and scientific support.

EA is supported by the Helmholtz Association under the joint research school “Munich School for Data Science - MUDS”.

References

1. Aitchison, J. The statistical analysis of compositional data. *J. Royal Stat. Soc. Ser. B (Methodological)* **44**, 139–160 (1982).
2. Blei, D. M. & Lafferty, J. D. Correlated topic models. *Adv. Neural Inf. Process. Syst.* 147–154 (2005).
3. Blei, D. M. & Lafferty, J. D. A correlated topic model of Science. *The Annals Appl. Stat.* **1**, 17–35, DOI: [10.1214/07-aos114](https://doi.org/10.1214/07-aos114) (2007). [arXiv:0708.3601v2](https://arxiv.org/abs/0708.3601v2).
4. Rozenblatt-Rosen, O., Stubbington, M. J., Regev, A. & Teichmann, S. A. The human cell atlas: from vision to reality. *Nat. News* **550**, 451 (2017).
5. Turnbaugh, P. J. *et al.* The human microbiome project. *Nature* **449**, 804–810 (2007).
6. Quinn, T. P., Erb, I., Richardson, M. F. & Crowley, T. M. Understanding sequencing data as compositions: an outlook and review. *Bioinformatics* **34**, 2870–2878, DOI: [10.1093/bioinformatics/bty175](https://doi.org/10.1093/bioinformatics/bty175) (2018).
7. Gloor, G. B., Macklaim, J. M., Pawlowsky-Glahn, V. & Egozcue, J. J. Microbiome datasets are compositional: and this is not optional. *Front. microbiology* **8**, 2224 (2017).
8. Johnson, J. S. *et al.* Evaluation of 16s rna gene sequencing for species and strain-level microbiome analysis. *Nat. communications* **10**, 1–11 (2019).
9. Rivera-Pinto, J. *et al.* Balances: a new perspective for microbiome analysis. *MSystems* **3**, e00053–18 (2018).
10. Bates, S. & Tibshirani, R. Log-ratio lasso: scalable, sparse estimation for log-ratio models. *Biometrics* **75**, 613–624 (2019).
11. Cammarota, G. *et al.* Gut microbiome, big data and machine learning to promote precision medicine for cancer. *Nat. Rev. Gastroenterol. Hepatol.* **17**, 635–648, DOI: [10.1038/s41575-020-0327-3](https://doi.org/10.1038/s41575-020-0327-3) (2020).
12. Quinn, T. P., Nguyen, D., Rana, S., Gupta, S. & Venkatesh, S. DeepCoDA: personalized interpretability for compositional health data. *arXiv* (2020). [2006.01392](https://arxiv.org/abs/2006.01392).
13. Oh, M. & Zhang, L. Deepmicro: deep representation learning for disease prediction based on microbiome data. *Sci. Reports* **10**, DOI: [10.1038/s41598-020-63159-5](https://doi.org/10.1038/s41598-020-63159-5) (2020).
14. Buettner, M., Ostner, J., Mueller, C. L., Theis, F. J. & Schubert, B. scCODA is a bayesian model for compositional single-cell data analysis. *Nat. communications* **12**, 6876 (2021).
15. Park, J., Yoon, C., Park, C. & Ahn, J. Kernel methods for radial transformed compositional data with many zeros. In *International Conference on Machine Learning*, 17458–17472 (PMLR, 2022).
16. Huang, S., Ailer, E., Kilbertus, N. & Pfister, N. Supervised learning and model analysis with compositional data. *PLOS Comput. Biol.* **19**, e1011240 (2023).
17. Taba, N., Fischer, K., research team, E. B., Org, E. & Aasmets, O. A novel framework for assessing causal effect of microbiome on health: long-term antibiotic usage as an instrument. *medRxiv* DOI: [10.1101/2023.09.20.23295831](https://doi.org/10.1101/2023.09.20.23295831) (2023). <https://www.medrxiv.org/content/early/2023/12/11/2023.09.20.23295831.full.pdf>.
18. K, X. *et al.* Causal Effects of Gut Microbiome on Systemic Lupus Erythematosus: A Two-Sample Mendelian Randomization Study. *Front. immunology* **12**, DOI: [10.3389/fimmu.2021.667097](https://doi.org/10.3389/fimmu.2021.667097)Format: (2021).
19. Arnold, K. F., Berrie, L., Tennant, P. W. & Gilthorpe, M. S. A causal inference perspective on the analysis of compositional data. *Int. journal epidemiology* **49**, 1307–1313 (2020).
20. Breskin, A. & Murray, E. J. Commentary: Compositional data call for complex interventions. *Int. J. Epidemiol.* **49**, 1314–1315 (2020).
21. Chapin, F. S. *et al.* Consequences of changing biodiversity. *Nature* **405**, 234–242, DOI: [10.1038/35012241](https://doi.org/10.1038/35012241) (2000).
22. Blaser, M. J. *Missing Microbes: How the Overuse of Antibiotics Is Fueling Our Modern Plagues* (Henry Holt and Company, New York, 2014), first edit edn.
23. Heumos, L. *et al.* Best practices for single-cell analysis across modalities. *Nat. Rev. Genet.* 1–23 (2023).

24. Shade, A. Diversity is the question, not the answer. *The ISME journal* **11**, 1–6 (2017).
25. Willis, A. Rarefaction, alpha diversity, and statistics. *Front. Microbiol.* **10**, 2407, DOI: [10.3389/fmicb.2019.02407](https://doi.org/10.3389/fmicb.2019.02407) (2019).
26. Kers, J. G. & Saccenti, E. The power of microbiome studies: Some considerations on which alpha and beta metrics to use and how to report results. *Front. Microbiol.* **12**, DOI: [10.3389/fmicb.2021.796025](https://doi.org/10.3389/fmicb.2021.796025) (2022).
27. Vujkovic-Cvijin, I. *et al.* Host variables confound gut microbiota studies of human disease. *Nat.* **2020** 1–7, DOI: [10.1038/s41586-020-2881-9](https://doi.org/10.1038/s41586-020-2881-9) (2020).
28. Sohn, M. B. & Li, H. Compositional mediation analysis for microbiome studies. *Annals Appl. Stat.* **13**, 661–681, DOI: [10.1214/18-AOAS1210](https://doi.org/10.1214/18-AOAS1210) (2019).
29. Carter, K. M., Lu, M., Jiang, H. & An, L. An information-based approach for mediation analysis on high-dimensional metagenomic data. *Front. Genet.* **11**, 148 (2020).
30. Wang, C., Hu, J., Blaser, M. J., Li, H. & Birol, I. Estimating and testing the microbial causal mediation effect with high-dimensional and compositional microbiome data. *Bioinformatics* DOI: [10.1093/bioinformatics/btz565](https://doi.org/10.1093/bioinformatics/btz565) (2020).
31. Xia, Y. Mediation analysis of microbiome data and detection of causality in microbiome studies. *Inflammation, Infect. Microbiome Cancers: Evidence, Mech. Implic.* 457–509 (2021).
32. Sohn, M. B., Lu, J. & Li, H. A compositional mediation model for a binary outcome: Application to microbiome studies. *Bioinformatics* **38**, 16–21 (2022).
33. Wang, C. *et al.* A microbial causal mediation analytic tool for health disparity and applications in body mass index. *Microbiome* **11**, 164, DOI: [10.1186/s40168-023-01608-9](https://doi.org/10.1186/s40168-023-01608-9) (2023).
34. Zhang, H. *et al.* Mediation effect selection in high-dimensional and compositional microbiome data. *Stat. Medicine* **40**, DOI: [10.1002/sim.8808](https://doi.org/10.1002/sim.8808) (2020).
35. Sommer, A. J. *et al.* A randomization-based causal inference framework for uncovering environmental exposure effects on human gut microbiota. *PLoS computational biology* **18**, e1010044 (2022).
36. Pearl, J. *Causality* (Cambridge university press, 2009).
37. Angrist, J. D. & Pischke, J.-S. *Mostly harmless econometrics: An empiricist's companion* (Princeton university press, 2008).
38. Hernán, M. A. & Robins, J. M. Instruments for causal inference: an epidemiologist's dream? *Epidemiology* 360–372 (2006).
39. Imbens, G. W. & Rubin, D. B. *Causal inference in statistics, social, and biomedical sciences* (Cambridge University Press, 2015).
40. Pearl, J. On the testability of causal models with latent and instrumental variables. In *Proceedings of the Eleventh conference on Uncertainty in artificial intelligence*, 435–443 (Morgan Kaufmann Publishers Inc., 1995).
41. Bonet, B. Instrumentality tests revisited. In *Proceedings of the 17th Conference on Uncertainty in Artificial Intelligence*, 48–55 (2001).
42. Gunsilius, F. Testability of instrument validity under continuous endogenous variables. *arXiv preprint arXiv:1806.09517* (2018).
43. Newey, W. K. & Powell, J. L. Instrumental variable estimation of nonparametric models. *Econometrica* **71**, 1565–1578 (2003).
44. Blundell, R., Chen, X. & Kristensen, D. Semi-nonparametric iv estimation of shape-invariant engel curves. *Econometrica* **75**, 1613–1669 (2007).
45. Singh, R., Sahani, M. & Gretton, A. Kernel instrumental variable regression. In *Advances in Neural Information Processing Systems*, 4593–4605 (2019).

46. Muandet, K., Mehrjou, A., Lee, S. K. & Raj, A. Dual instrumental variable regression. *arXiv preprint arXiv:1910.12358* (2019).
47. Zhang, R., Imaizumi, M., Schölkopf, B. & Muandet, K. Maximum moment restriction for instrumental variable regression. *arXiv preprint arXiv:2010.07684* (2020).
48. Bennett, A. *et al.* Minimax instrumental variable regression and l2 convergence guarantees without identification or closedness. *arXiv preprint arXiv:2302.05404* (2023).
49. Rothenhäusler, D., Meinshausen, N., Bühlmann, P. & Peters, J. Anchor regression: Heterogeneous data meet causality. *J. Royal Stat. Soc. Ser. B: Stat. Methodol.* **83**, 215–246 (2021).
50. Pfister, N. & Peters, J. Identifiability of sparse causal effects using instrumental variables. In *Uncertainty in Artificial Intelligence*, 1613–1622 (PMLR, 2022).
51. Ailer, E., Hartford, J. & Kilbertus, N. Sequential underspecified instrument selection for cause-effect estimation. In *Proceedings of the 40th International Conference on Machine Learning*, vol. 202 of *Proceedings of Machine Learning Research*, 408–420 (PMLR, 2023).
52. Kelejian, H. H. Two-stage least squares and econometric systems linear in parameters but nonlinear in the endogenous variables. *J. Am. Stat. Assoc.* **66**, 373–374 (1971).
53. Pawlowsky-Glahn, V. & Egozcue, J. J. Geometric approach to statistical analysis on the simplex. *Stoch. Environ. Res. Risk Assess.* **15**, 384–398 (2001).
54. Egozcue, J. J., Pawlowsky-Glahn, V., Mateu-Figueras, G. & Barcelo-Vidal, C. Isometric logratio transformations for compositional data analysis. *Math. Geol.* **35**, 279–300 (2003).
55. Greenacre, M. & Grunsky, E. The isometric logratio transformation in compositional data analysis: a practical evaluation. *preprint* (2019).
56. Aitchison, J. & Bacon-Shone, J. Log contrast models for experiments with mixtures. *Biometrika* **71**, 323–330, DOI: [10.1093/biomet/71.2.323](https://doi.org/10.1093/biomet/71.2.323) (1984).
57. Lin, W., Shi, P., Feng, R. & Li, H. Variable selection in regression with compositional covariates. *Biometrika* **101**, 785–797, DOI: [10.1093/biomet/asu031](https://doi.org/10.1093/biomet/asu031) (2014).
58. Shi, P., Zhang, A. & Li, H. Regression analysis for microbiome compositional data. *The Annals Appl. Stat.* **10**, 1019 – 1040, DOI: [10.1214/16-AOAS928](https://doi.org/10.1214/16-AOAS928) (2016).
59. Combettes, P. & Müller, C. Regression models for compositional data: General log-contrast formulations, proximal optimization, and microbiome data applications. *Stat. Biosci.* DOI: [10.1007/s12561-020-09283-2](https://doi.org/10.1007/s12561-020-09283-2) (2021).
60. Combettes, P. L. & Müller, C. L. Perspective maximum likelihood-type estimation via proximal decomposition. *Electron. J. Stat.* **14**, 207 – 238, DOI: [10.1214/19-EJS1662](https://doi.org/10.1214/19-EJS1662) (2020).
61. Kaul, A., Mandal, S., Davidov, O. & Peddada, S. D. Analysis of microbiome data in the presence of excess zeros. *Front. microbiology* **8**, 2114 (2017).
62. Lin, H. & Peddada, S. D. Analysis of microbial compositions: a review of normalization and differential abundance analysis. *NPJ biofilms microbiomes* **6**, 1–13 (2020).
63. Shi, P., Zhou, Y. & Zhang, A. R. High-dimensional log-error-in-variable regression with applications to microbial compositional data analysis. *Biometrika* **109**, 405–420 (2022).
64. Leinster, T. & Cobbold, C. Measuring diversity: The importance of species similarity. *Ecology* **93**, 477–89, DOI: [10.2307/23143936](https://doi.org/10.2307/23143936) (2012).
65. Chao, A., Chiu, C.-H. & Jost, L. Unifying species diversity, phylogenetic diversity, functional diversity, and related similarity and differentiation measures through hill numbers. *Annu. review ecology, evolution, systematics* **45**, 297–324 (2014).

66. Daly, A. J., Baetens, J. M. & De Baets, B. Ecological diversity: measuring the unmeasurable. *Mathematics* **6**, 119 (2018).
67. Bello, M. G. D., Knight, R., Gilbert, J. A. & Blaser, M. J. Preserving microbial diversity. *Science* DOI: [10.1126/science.aau8816](https://doi.org/10.1126/science.aau8816) (2018).
68. Greene, W. H. Accounting for excess zeros and sample selection in poisson and negative binomial regression models. *NYU working paper no. EC-94-10* (1994).
69. Xu, L., Paterson, A. D., Turpin, W. & Xu, W. Assessment and selection of competing models for zero-inflated microbiome data. *PloS one* **10**, e0129606 (2015).
70. Hartford, J., Lewis, G., Leyton-Brown, K. & Taddy, M. Deep iv: A flexible approach for counterfactual prediction. In *International Conference on Machine Learning*, 1414–1423 (2017).
71. Bennett, A., Kallus, N. & Schnabel, T. Deep generalized method of moments for instrumental variable analysis. In Wallach, H. *et al.* (eds.) *Advances in Neural Information Processing Systems*, vol. 32 (Curran Associates, Inc., 2019).
72. Andrews, I., Stock, J. H. & Sun, L. Weak instruments in instrumental variables regression: Theory and practice. *Annu. Rev. Econ.* **11**, 727–753 (2019).
73. Sanderson, E. & Windmeijer, F. A weak instrument f-test in linear iv models with multiple endogenous variables. *J. Econom.* **190**, 212–221, DOI: <https://doi.org/10.1016/j.jeconom.2015.06.004> (2016). Endogeneity Problems in Econometrics.
74. Schulfer, A. *et al.* The impact of early-life sub-therapeutic antibiotic treatment (stat) on excessive weight is robust despite transfer of intestinal microbes. *The ISME J.* **13**, 1, DOI: [10.1038/s41396-019-0349-4](https://doi.org/10.1038/s41396-019-0349-4) (2019).
75. Rubin, D., Imbens, G. & Angrist, J. Identification of causal effects using instrumental variables: Rejoinder. *J. Am. Stat. Assoc.* **91**, DOI: [10.2307/2291629](https://doi.org/10.2307/2291629) (1993).
76. Kilbertus, N., Kusner, M. J. & Silva, R. A class of algorithms for general instrumental variable models. In *Advances in Neural Information Processing Systems*, vol. 33 (2020).
77. van Rossum, G. & Drake, F. L. *Python 3 Reference Manual* (CreateSpace, 2009).
78. Inc., P. T. Collaborative data science (2015).
79. Harris, C. R. *et al.* Array programming with NumPy. *Nature* (2020).
80. Wes McKinney. Data Structures for Statistical Computing in Python. In Stéfan van der Walt & Jarrod Millman (eds.) *Proceedings of the 9th Python in Science Conference*, 56 – 61, DOI: [10.25080/Majora-92bf1922-00a](https://doi.org/10.25080/Majora-92bf1922-00a) (2010).
81. Pedregosa, F. *et al.* Scikit-learn: Machine learning in Python. *JMLR* (2011).
82. scikit-bio development team, T. scikit-bio: A bioinformatics library for data scientists, students, and developers (2020).
83. Gautier, L. (2021).
84. Hunter, J. D. Matplotlib: A 2D graphics environment. *Comput. Sci. & Eng.* (2007).
85. Seabold, S. & Perktold, J. statsmodels: Econometric and statistical modeling with python. In *9th Python in Science Conference* (2010).
86. pandas development team, T. pandas-dev/pandas: Pandas, DOI: [10.5281/zenodo.3509134](https://doi.org/10.5281/zenodo.3509134) (2020).
87. Bradbury, J. *et al.* JAX: Composable transformations of Python+NumPy programs (2018).
88. Suh, E. J. (2020).
89. Simpson, L., Combettes, P. & Müller, C. c-lasso - a python package for constrained sparse and robust regression and classification. *J. Open Source Softw.* **6**, 2844, DOI: [10.21105/joss.02844](https://doi.org/10.21105/joss.02844) (2021).
90. R Core Team. *R: A Language and Environment for Statistical Computing*. R Foundation for Statistical Computing, Vienna, Austria (2020).

91. Kurtz, Z. D., Bonneau, R. & Müller, C. L. Disentangling microbial associations from hidden environmental and technical factors via latent graphical models. *bioRxiv* DOI: [10.1101/2019.12.21.885889](https://doi.org/10.1101/2019.12.21.885889) (2019).
92. Oksanen, J. *et al.* *vegan: Community Ecology Package* (2020). R package version 2.5-7.
93. Tsagris, M. & Athineou, G. *Compositional: Compositional Data Analysis* (2021). R package version 4.5.
94. Patuzzi, I., Baruzzo, G., Losasso, C., Ricci, A. & Di Camillo, B. metasparsim: a 16s rrna gene sequencing count data simulator. *BMC Bioinforma.* **20**, DOI: [10.1186/s12859-019-2882-6](https://doi.org/10.1186/s12859-019-2882-6) (2019).

Author contributions statement

NK, CLM and EA wrote the manuscript. NK and CLM reviewed the manuscript. EA conducted the analysis.

Additional Information

No competing interest is declared.

S1 Supplementary Material

The supplementary material contains details on compositional data transformations (Supplementary Material S2) and the applied instrumental variables methods (Supplementary Material S3) as well as a list of the packages that have been used in the implementation (Supplementary Material S4). Further, the supplementary material provides additional results for the real data example of [74] (Supplementary Material S5). Moreover for the synthetic settings it holds a detailed description of the data generation (Supplementary Material S6), the parameter settings for the training of the methods (Supplementary Material S7) as well as additional results and visualizations (Supplementary Material S8).

S2 Compositional Data Transformations

Given a compositional vector $x \in \mathbb{S}^{p-1}$, the definitions of the log-transformations are given by the additive log-ratio transformation

$$\text{alr}(x) := \left(\log \frac{x_1}{x_p}, \dots, \log \frac{x_{p-1}}{x_p} \right) = \tilde{x}_{\text{alr}} = \log(x) \cdot \begin{bmatrix} 1 & 0 & \dots & 0 \\ 0 & 1 & \dots & 0 \\ \vdots & \vdots & \ddots & \vdots \\ 0 & 0 & \dots & 1 \\ -1 & -1 & \dots & -1 \end{bmatrix} \quad (8)$$

with inverse

$$\text{alr}^{-1}(\tilde{x}) = C(\exp([\tilde{x}, 0])), \quad (9)$$

the centered log-ratio transformation

$$\text{clr}(x) := \left(\log \frac{x_1}{g(x)}, \dots, \log \frac{x_p}{g(x)} \right) = \tilde{x}_{\text{clr}} = \frac{\log(x)}{D} \cdot \begin{bmatrix} D-1 & -1 & \dots & -1 \\ -1 & D-1 & \dots & -1 \\ \vdots & \vdots & \ddots & \vdots \\ -1 & -1 & \dots & D-1 \end{bmatrix} \quad (10)$$

with $g(x) := \sqrt[p]{x_1 \cdot \dots \cdot x_p}$ and inverse

$$\text{clr}^{-1}(\tilde{x}) = C(\exp([\tilde{x}])), \quad (11)$$

and the isometric log-ratio transformation

$$\text{ilr}_V(x) = \tilde{x}_{\text{ilr}} = \text{clr}(x) \cdot V \quad (12)$$

for a matrix $V \in \mathbb{R}^{p \times p-1}$ such that $V^T V = \mathbb{I}_{p-1}$ providing an orthonormal basis of \mathbb{R}^{p-1} with inverse

$$\text{ilr}_V^{-1}(\tilde{x}) = C(\exp([\tilde{x}V^T])). \quad (13)$$

For the ilr transformation, a typical choice for V^T is the so-called Helmert matrix with the first row removed (see for example <http://scikit-bio.org/docs/0.4.1/generated/generated/skbio.stats.composition.ilr.html>).

S3 IV Methods

We consider three different approaches that gradually relax some of the common IV assumptions. In particular, the restrictions on the function space of f are gradually relaxed in the different settings.

The Two-Stage Least Squares algorithm (2SLS) consists of two sequential OLS regressions [75]. 2SLS is one of the most prominent approaches. It allows for unobserved confounding while still putting linear restrictions on the function space of f and assuming additive noise:

$$Y = \beta X + \varepsilon_Y \quad (14)$$

First, 2SLS fits a regression model based on Z to predict X . The second stage uses the estimated \hat{X} to predict Y . This results in the following estimator for β :

$$\hat{\beta} = (X^T P_Z X)^{-1} (X^T P_Z Y) \quad (15)$$

with $P_Z = Z(Z^T Z)^{-1} Z^T$.

If $p = q$, the estimator reduces to the following form:

$$\hat{\beta} = (Z^T X)^{-1} (Z^T y) \quad (16)$$

[45] relax the assumption of the linear setting in 2SLS towards a non-parametric generalization of the causal effect by applying kernel ridge regression (KIV).

$$Y = f(X) + \varepsilon_Y, \quad (17)$$

for a potentially non-linear f , maintaining the additive noise assumption for point-identifiability.

The OLS regressions are replaced by kernel ridge regressions and thus model the relationship of Z , X and Y by non-linear functions in reproducing kernel Hilbert spaces (RKHSs). This method still requires additive noise models to produce consistent results. Following the arguments in [45], this gives us a closed form solution for f :

$$W = K_{XX} (K_{ZZ} + n\lambda Id)^{-1} K_{ZZ} \quad (18)$$

$$\hat{\alpha} = (W W^T + m\xi K_{XX})^{-1} W \tilde{y}, \quad (19)$$

$$\hat{f}_\xi^m(x) = (\hat{\alpha})^T K_{Xx} \quad (20)$$

In the next step, we drop the assumption of additive noise, i.e., allowing $f(X, U)$ to depend on the treatment X and any (potentially high-dimensional) confounder U in arbitrary ways (also non-linearly). This implies that the effect is only partially identifiable, i.e., we can only put lower and upper bounds on $\mathbb{E}[Y | do(x)]$. The authors in [76] employ the response function framework to minimize (maximize) the average causal effect over all causal models that satisfy the structural IV assumptions and simultaneously match the observed data to find the lower (upper) bound. We refer the reader to the original paper for the details [76].

S4 Package References

Here, we briefly outline the software used in our empirical evaluation. Please note that the code and the requirements are all available at <https://github.com/EAILer/causal-compositions>.

Python Packages

We use the following Python [77] packages: Plotly [78], Numpy [79], Scipy [80], scikit-learn [81], scikit-bio [82], rpy2 [83], Matplotlib [84], Statsmodels [85], Pandas [86], Jax [87], Dirichlet [88], c-Lasso [89].

R Packages

We use the following R [90] packages: SpiecEasi [91], vegan [92], Compositional [93] and metaSparSim [94].

S5 Case study on murine sub-therapeutic antibiotic treatment

In this part we turn to the analysis of the microbiome instead of the summary statistic as the cause. This is a more detailed examination of the murine sub-therapeutic antibiotic treatment data given in the main part. We provide results on higher aggregation levels, i.e., the taxonomic ranks ‘Order’ and ‘Family’, respectively. Moreover, we discretize the weight outcome Y and replace the squared loss of the log-contrast regression by a Hinge loss (see Supplementary Material S7).

—*Further Results on different Aggregation Levels:* Naturally, for real data, we do not have ground truth labels available. However, the importance of being able to draw causal and actionable conclusions becomes apparent. In the main part we provide the results for the naive regression and the two-stage method ILR+LC on genus level. The methods did not agree on the influential log-ratios, thus suggesting that Only LC might be subject to confounding. This result also holds true on family level. However, on order level both methods detect one common log-ratio (see Figure S1).

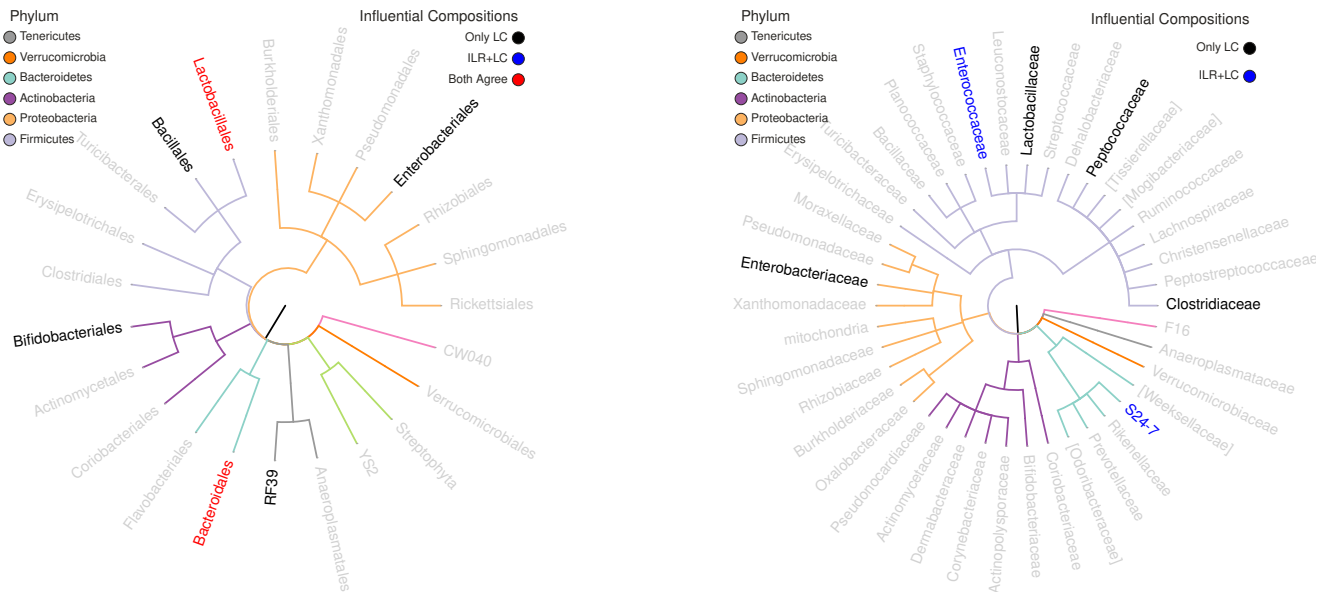


Figure S1. Influential Compositions on Order Level (left) and Family Level (right): On order level, both methods agree on one influential log ratio. For the family level, there is a divide between the two-stage method and the naive regression. This could suggest that Only LC is subject to confounding on the corresponding aggregation level.

—*Categorical/Binary Outcome:* In order to provide a more complete picture of the loss possibilities, we include results for a categorical/binary Y . Originally, the real data includes weight measured in gram. To create a binary outcome, we split the data by the mean of the outcome Y thus artificially generating an “underweight” population of 29 mice and an “overweight” population of 28 mice. Again, we show the influential log-ratios for the naive regression Only LC and ILR+LC (see Figure S2). While for ILR+LC the influential log-ratios stay the same for binary and continuous outcome, for the naive regression they are not entirely consistent.

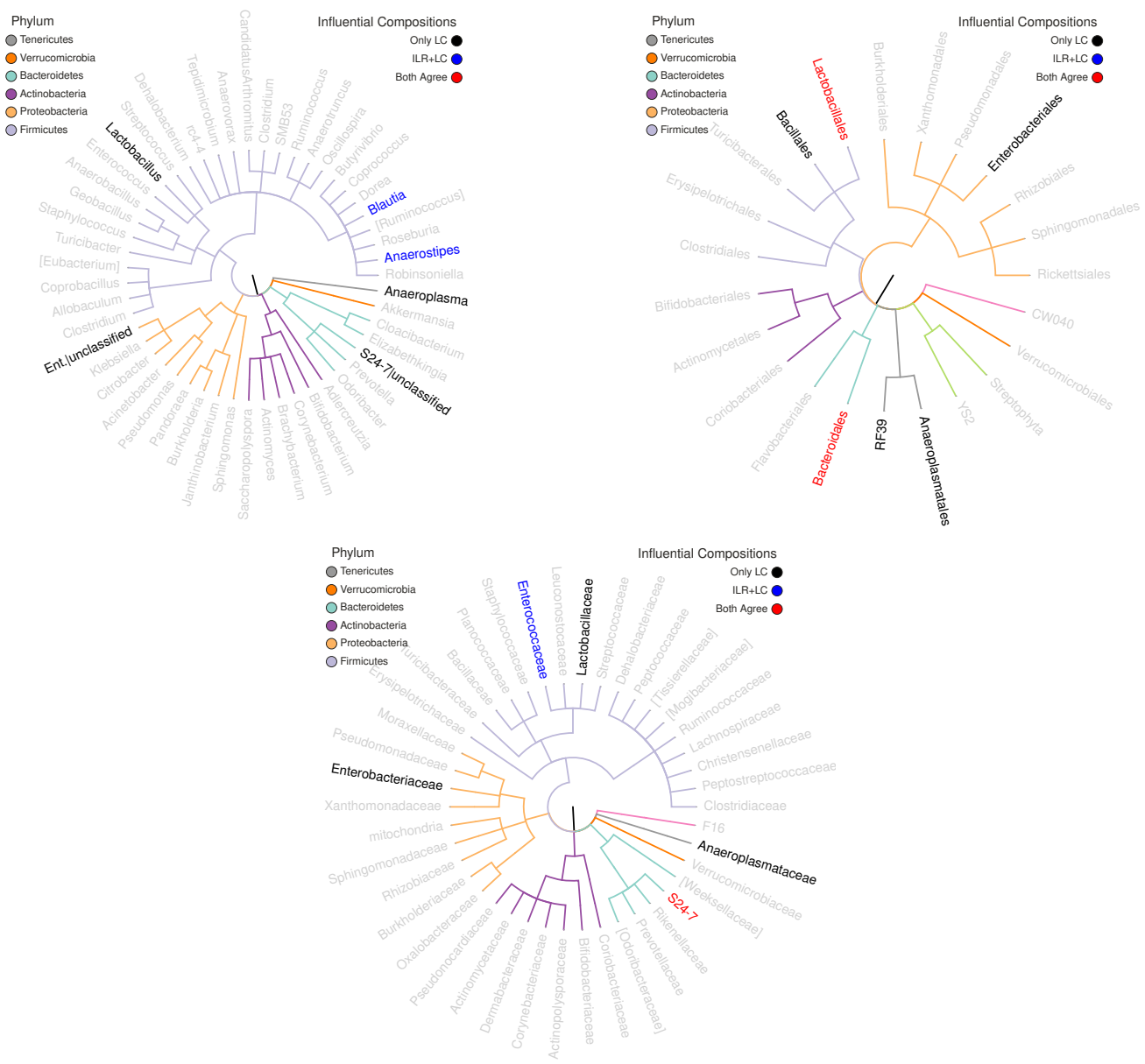


Figure S2. Influential Compositions on Genus Level (top left), Order Level (top right) and Family Level (bottom): In general, the results stay the same for ILR+LC in the binary case and the continuous case. The influential log-ratios are slightly shifting when simply applying a naive regression.

S6 Data Generation

This section describes the details of how we generate data for our empirical evaluation. Complementary to the real microbiome data, we consider several approaches to generate data for the compositional instrumental variable setting. Since counterfactuals are never observed in practice, we need a setup where the ground truth is known and can be controlled. We choose to simulate data from two different data generating models, Setting A and Setting B. The first one will put (most of) our models in a wellspecified setting, where we have strong expectations and theoretical guarantees on how they will behave. The other approach simulates compositional data by a zero-inflated negative binomial. Thus, the first stage of all of our models will be misspecified (except for potentially KIV assuming a proper choice of the kernels). This allows us to test our models for robustness and probe their limitations.

Based on this motivation, we also describe two additional parameter settings within Setting A that will examine robustness and limitations: a weak instrument scenario and a scenario with a non-linear second stage f . The first scenario will test the necessity of a strong/valid instrument, the second scenario will further look into the issue of misspecification (now in the second stage).

We describe the data generating model and the specific parameter settings. We also provide visualizations of the resulting data distributions, which is rather tricky for compositional data with $p > 3$. We will then supplement the result section of the main text with additional comments on the evaluation of the results and show the complete set of plots for Tables 1 and 2.

Each generated dataset for $p = 3$ comprises $n = 1000$ samples, resp. 10,000 samples for $p = 30$ and $p = 250$, with an additional $n_{\text{intervention}} = 250$ interventional samples for evaluation of OOS MSE. Note that the examples in the figures show only one of these datasets. To ensure reproducibility, we consistently chose the 10th dataset of the confidence runs for (a representative) visualization.

Setting A

The following explanations refer to *Setting A* described in the main part.

Setting A generates data that enables us to assess our methods in a *wellspecified* setting. Instead of modeling $X \in \mathbb{S}^{p-1}$ directly, we model $\text{ilr}(X)$. The setting is strictly linear in $\text{ilr}(X)$. This means that both g and f are linear functions of U and Z , resp., U and $\text{ilr}(X)$. The generative model is as follows:

$$\begin{aligned} Z_j &\sim \text{Uniform}(0, 1) \\ U &\sim \mathcal{N}(\mu_c, 1) \\ \text{ilr}(X) = g(Z, U) &= \alpha_0 + \alpha Z + c_X U \\ Y = f(X, U) &= \beta_0 + \beta^T \text{ilr}(X) + c_Y U \end{aligned} \quad (21)$$

Setting A with $p = 3, q = 2$

The main characteristics of this lower dimensional dataset are the presence of all microbes and relatively seldom zero values. We choose the following parameters for the low-dimensional case:

$$\mu_c = -3, \alpha_0 = [1, 1], \alpha = \begin{bmatrix} 0.5 & -0.15 \\ 0.3 & 0.7 \end{bmatrix}, c_X = [0.5, 0.5], \beta_0 = 0.5, \beta = [4, 1], c_Y = 4 \quad (22)$$

The first stage F-test for the two components of $\text{ilr}(X)$ gives (32.18, 113.99) for the 10th data sample.

We remark that in higher dimensions, the F-test does not provide a strong theoretical justification for sufficient instrument strength, but we still use it as a sensible heuristic that provides a relative measure between different settings, i.e., in which scenario the instrument is stronger.

For the $p = 3$ case, we can visualize X by its compositional coordinates not only in a barplot (Figure S3) but also in an arguably more informative ternary plot (Figure S4). To visualize the linear relationship between observed $\text{ilr}(X)$ and Y as well as the true effect $Y | do(X)$, we transform the data X and visualize each component in a separate scatter plot (see Figure S5).

Setting A with $p = 30, q = 10$

Contrary to the previous example, we now analyze a slightly higher-dimensional setting with $p = 30$. In this scenario, it makes sense to introduce sparsity in the data generation process from a practical viewpoint. We work with the data generation setting given in Equation (21) and choose the following parameters:

$$\begin{aligned} \mu_c &= 5, \alpha_0 = [3, 1, 1, 1, 3, 1, 1, 1, 0, \dots, 0], \alpha_{ij} \begin{cases} 0, & \text{for } i \neq j \text{ and } i, j > 8, \\ 1, & \text{for } i \neq j \leq 8 \end{cases}, \\ c_X &= [-2, -1, -1, -1, 2, 1, 1, 1, 0, \dots, 0], \beta_0 = 5, \beta_{\log} = [10, 5, 5, 5, -10, -5, -5, -5, 0, \dots, 0], \beta = V^T \cdot \beta_{\log}, c_Y = 5 \end{aligned}$$

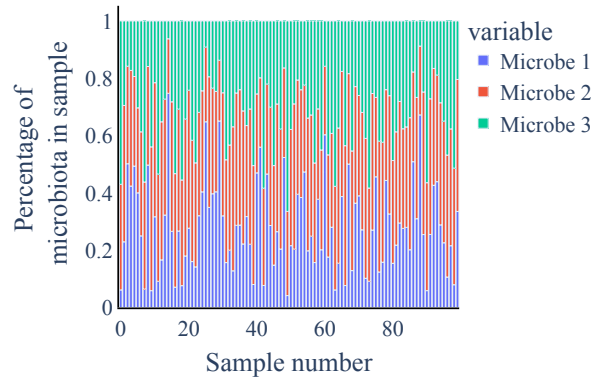


Figure S3. Setting A with $p = 3, q = 2$: The barplot shows the three-part composition of the first 100 samples. The microbes are evenly distributed over the individual compositions.

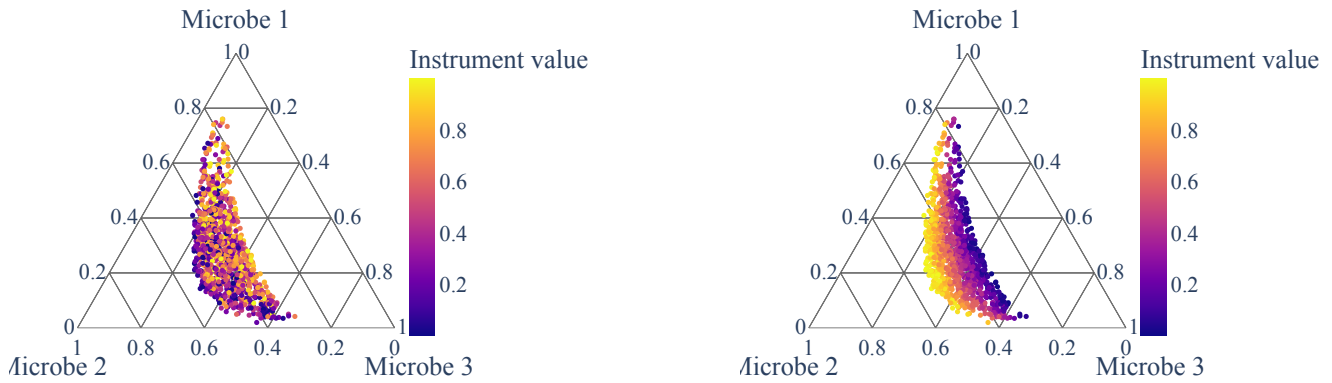


Figure S4. Setting A with $p = 3, q = 2$: The ternary plots are colored by first (left) and second (right) instrument value. The influence of Z_2 on the composition X is particularly pronounced and visually supports the assumption of Z being a valid instrument.

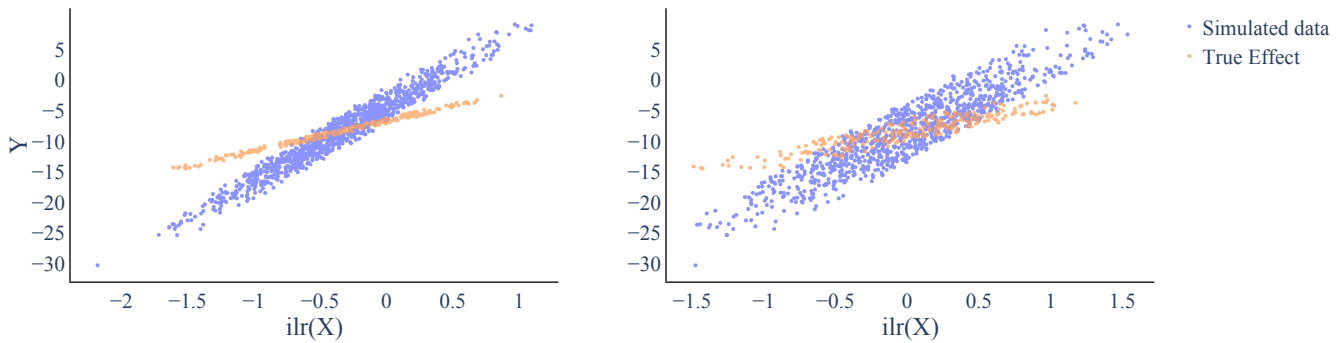


Figure S5. Setting A with $p = 3, q = 2$: Both plots show one component of $\text{ilr}(X) \in \mathbb{R}^2$ vs. the confounded outcome (blue) and the true effect (orange). Due to the confounding, the observed and the causal effect do not overlap. However, we expect the instrument Z to factor out the confounding effect and enable the two-stage methods to identify the causal effect.

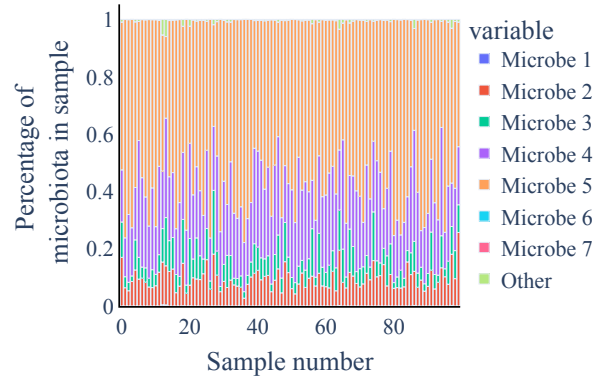


Figure S6. Setting A with $p = 30, q = 10$: The barplot shows the composition of the first 100 samples. The compositions are dominated by a few species.

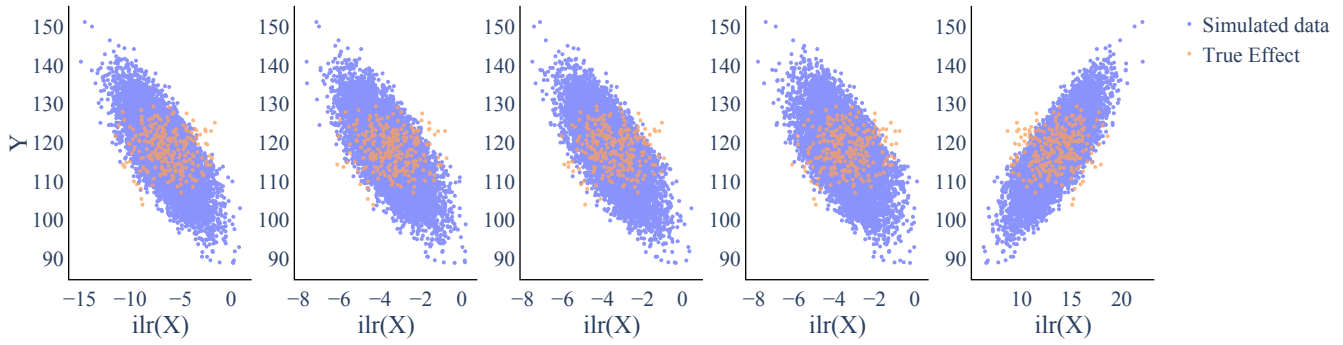


Figure S7. Setting A with $p = 30, q = 10$: Both plots show one component of $\text{ilr}(X) \in \mathbb{R}^{29}$ vs. the confounded outcome (blue) and the true effect (orange). Due to the confounding, the observed and the causal effect do not overlap. However, we expect the instrument Z to factor out the confounding effect and enable the two-stage methods to identify the causal effect.

for $i \in \{1, \dots, p-1\}, j \in \{1, \dots, q\}$ and V providing the orthonormal basis for the ilr-transformation (see Supplementary Material S2).

Since a visualization with a ternary plot is no longer feasible, we only show barplots of the data in Figure S6. However, scatter plots showing individual $\text{ilr}(X)$ coordinates versus the observed Y and the true causal effect are still informative. Since the first components are the most influential ones in our setting, we show the first five $\text{ilr}(X)$ components in Figure S7.

Setting A with $p = 250, q = 10$

We now analyze the second high-dimensional setting with $p = 250$. As in the scenario of $p = 30$, it makes sense to introduce sparsity in the data generation process from a practical viewpoint. We work with the data generation setting given in Equation (21) and choose the following parameters:

$$\mu_c = 3, \alpha_0 = [1, 1, 3, 1, 1, 1, 3, 1, 1, 1, 3, 1, 0, \dots, 0], \alpha_{ij} \begin{cases} 0, & \text{for } i \neq j \text{ and } i, j > 8, \\ 1, & \text{for } i \neq j \leq 8 \end{cases},$$

$$c_X = [-1, 2, -1, 2, -1, 2, -2, 1, -2, 1, -2, 1, 0, \dots, 0], \beta_0 = 5, \beta_{\log} = [10, 5, 5, 5, -10, -5, -5, -5, 0, \dots, 0],$$

$$\beta = V^T \cdot \beta_{\log}, c_Y = 5$$

for $i \in \{1, \dots, p-1\}, j \in \{1, \dots, q\}$ and V providing the orthonormal basis for the ilr-transformation (see Supplementary Material S2). Since a visualization with a ternary plot is no longer feasible, we only show barplots of the data in Figure S8. However, scatter plots showing individual $\text{ilr}(X)$ coordinates versus the observed Y and the true causal effect are still informative. Since the first components are the most influential ones in our setting, we show the first five $\text{ilr}(X)$ components in Figure S9.

Setting B

The following explanations refer to *Setting B* described in the main part.

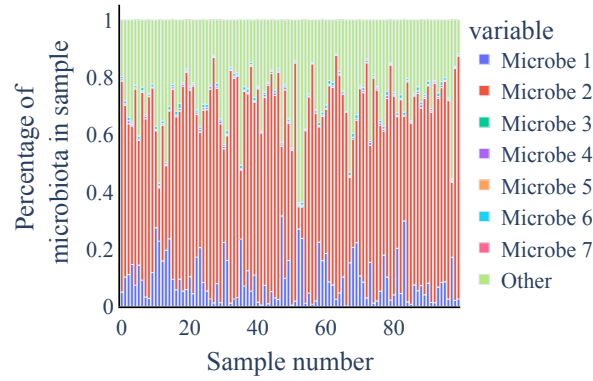


Figure S8. Setting A with $p = 250, q = 10$: The barplot shows the composition of the first 100 samples. The compositions are dominated by a few species.

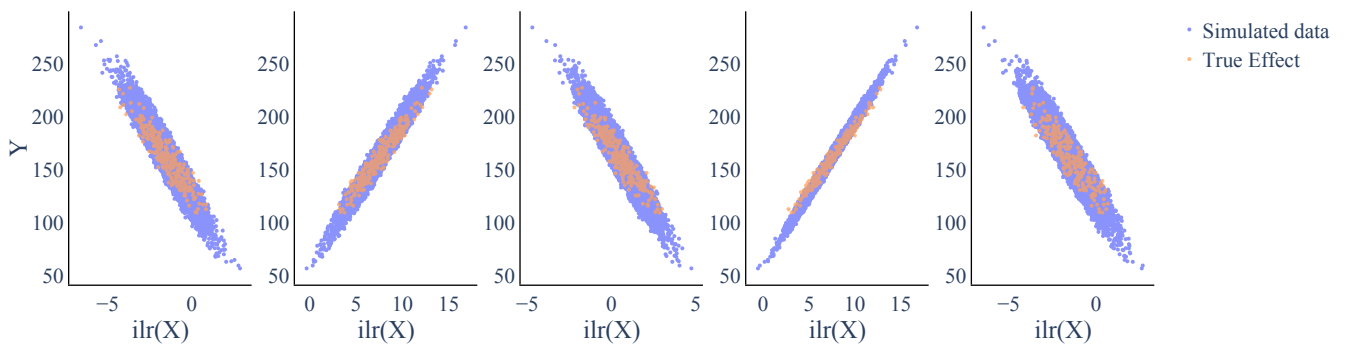


Figure S9. Setting A with $p = 250, q = 10$: Both plots show one component of $\text{ilr}(X) \in \mathbb{R}^{249}$ vs. the confounded outcome (blue) and the true effect (orange). Due to the confounding, the observed and the causal effect do not overlap. However, we expect the instrument Z to factor out the confounding effect and enable the two-stage methods to identify the causal effect.

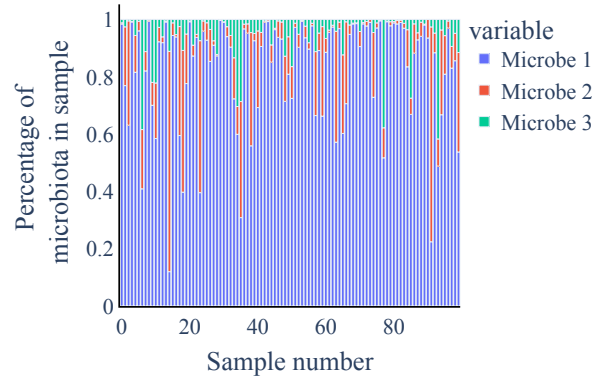


Figure S10. Setting B with $p = 3, q = 2$: The barplot shows the three-part composition of the first 100 samples. The data sample shows some dominating species in the individual compositions while having more variation between the samples compared to Setting A.

Setting B serves three main purposes: (i) to assess our methods on a dataset that closely resembles real-world data in terms of its distribution, (ii) to assess our methods when the first stage is misspecified, and (iii) to allow for sparsity in the first stage of the data generating process, resembling the real data in [74]. The sparsity of the compositional data can be accomplished by a zero-inflated negative binomial distribution. As ZINegBinomial is a frequently used distribution in modeling microbiome data, we assume a closer resemblance to real world sparsity than the resemblance we achieve in Setting A for $p = 30$ and $p = 250$.

The data is generated according to the following model with the parameter μ of the negative binomial as $\mu = \alpha_0 + \alpha Z$:

$$\begin{aligned}
 Z_j &\sim \text{Uniform}(Z_{\min}, Z_{\max}), \\
 U &\sim \text{Uniform}(U_{\min}, U_{\max}), \\
 X &= g(Z, U) \sim C(\text{ZINegBinomial}(\mu, \Sigma, \theta, \eta)) \oplus (\Omega_C \odot U), \\
 Y &= f(X, U) = \beta_0 + \beta^T \log(X) + c_Y^T \log(\Omega_C \odot U)
 \end{aligned} \tag{23}$$

We fix $Z_{\min} = 1, Z_{\max} = 10$ and $U_{\min} = 0.2, U_{\max} = 3$ throughout. For the negative binomial distribution we set $\Sigma = \mathbb{I}_p$, i.e., assuming no additional correlation within the different components of the composition for simplicity.

Setting B with $p = 3, q = 2$

The parameter setting with $p = 3$ does not yet contain sparse data due to its low-dimensionality. It serves the purpose to compare the performance of the two-stage methods in a misspecified setting and a wellspecified setting (except for DIR+LC which is misspecified in both Setting A and Setting B).

Here, we consider the following generative model based on Equation (23). We fix $Z_{\min} = 0, Z_{\max} = 10, U_{\min} = 0.2, U_{\max} = 3$.

We chose α_0 to be $[7, 9, 8]$ and $\alpha = \begin{bmatrix} 5 & 0 & 0 \\ 0 & 5 & 0 \\ 0 & 0 & 5 \end{bmatrix}$ to guarantee for valid instruments. We set the dispersion to $\theta = 2$ and keep the

zero probability at $\eta = [0, 0, 0]$ to get valid compositions for this low-dimensional scenario. For the confounding composition Ω_C , we set it to $[0.7, 0.1, 0.2]$. For the second stage, we fix ground truth parameters $\beta_0 = 1, \beta_{\log} = [-5, 3, 2]$, which results in $\beta = V^T \beta_{\log}$ and the confounding parameter $c_Y = [2, -10, -10]$.

The first stage F-test for the two components of $\text{ilr}(X)$ gives $(41.38, 14.08)$ for the 10th data sample. We remark that in higher dimensions, the F-test does not provide a strong theoretical justification for sufficient instrument strength, but we still use it as a sensible heuristic that provides a relative measure between different settings, i.e., in which scenario the instrument is stronger.

For the $p = 3$ case, we can visualize X by its compositional coordinates not only in a barplot (Figure S10) but also in an arguably more informative ternary plot (Figure S11). To visualize the relationship between observed $\text{ilr}(X)$ and Y as well as the true effect $Y \mid do(X)$, we transform the data X and visualize each component in a separate scatter plot (see Figure S12).

Setting B with $p = 30, q = 10$

In the higher-dimensional scenarios we will make use of the sparsity ability of the ZINegBinom distribution.

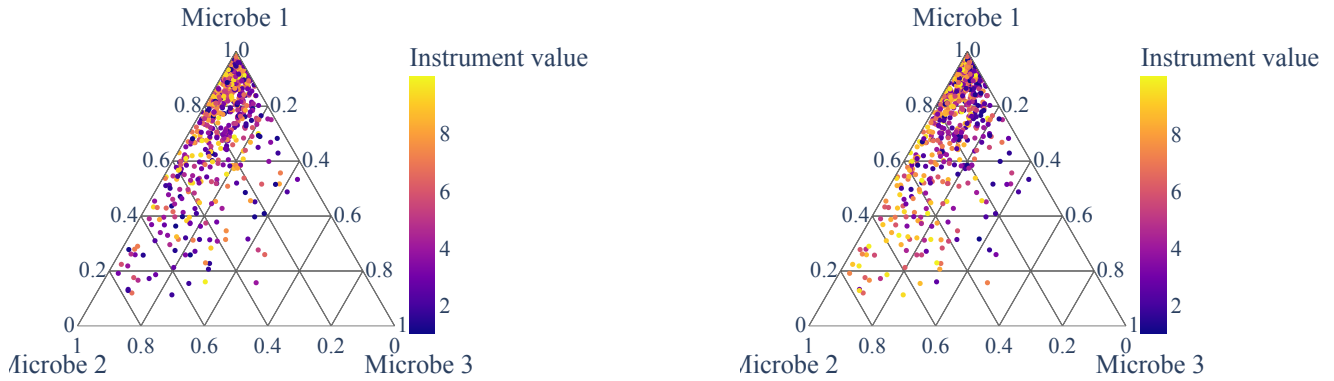


Figure S11. Setting B with $p = 3, q = 2$: The ternary plots are colored by first (left) and second (right) instrument value. Due to the data generation process, the influence of Z_1 and Z_2 on the composition X is less visually obvious than for Setting A. Nevertheless, Z can be assumed to be a valid instrument.

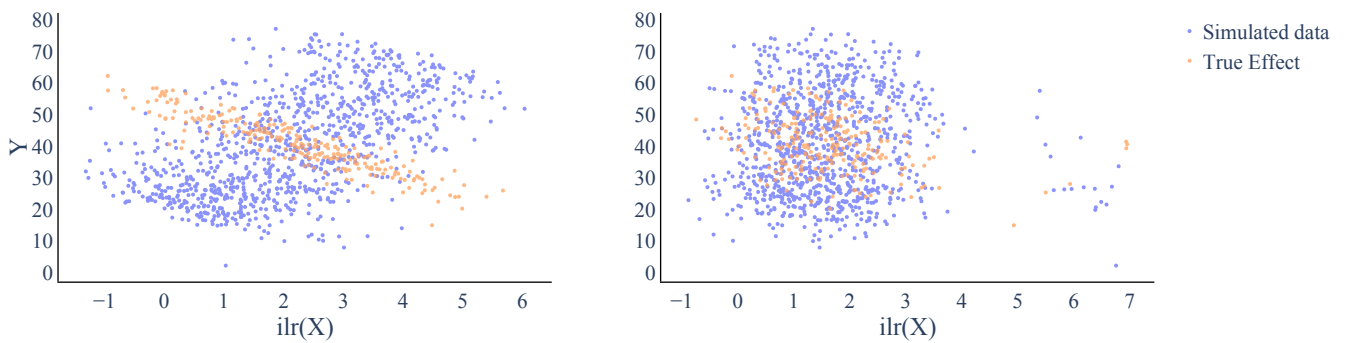


Figure S12. Setting B with $p = 3, q = 2$: Both plots show one component of $\text{ilr}(X) \in \mathbb{R}^2$ vs. the confounded outcome (blue) and the true effect (orange). Due to the confounding, the observed and the causal effect do not overlap. However, we expect the instrument Z to factor out the confounding effect and enable the two-stage methods to identify the causal effect.

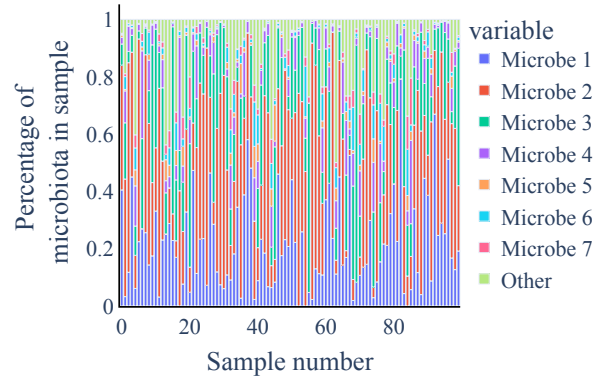


Figure S13. Setting B with $p = 30, q = 10$: The barplot shows the different compositions of the first 100 samples in the dataset. We observe some dominating components and many small components with an overall high variability.

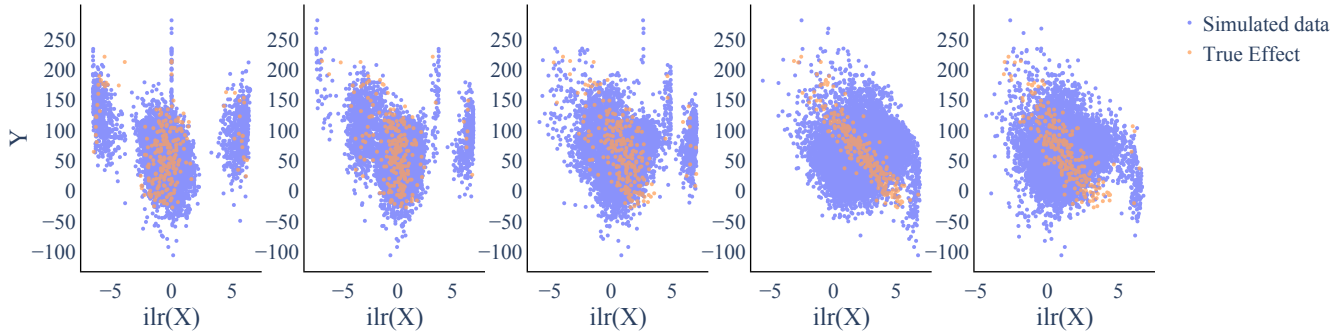


Figure S14. Setting B with $p = 30, q = 10$: Each plot shows one of the first five components of $\text{ilr}(X) \in \mathbb{R}^{29}$ vs. the confounded outcome (blue) and the true effect (orange). The dataset shows strong confounding in some of the components as the true effect and the observed effect actually contradict each other. We expect the two-stage methods to perform better than the naive regression in such scenarios. We can thus check if the two-stage methods are still able to make use of the instrument Z despite the misspecified first stage.

The parameters were chosen to generate a suitable dataset that still conveys typical compositional data properties (sparsity, high variance within the composition, similar means to real data) and significant instruments. Here, we consider the following generative model based on Equation (23). We fix $Z_{\min} = 0, Z_{\max} = 10, U_{\min} = 0.2, U_{\max} = 3$. To ensure a handful of components dominating the composition, we fix the first 8 entries of α_0 to be $[1, 1, 2, 1, 4, 4, 2, 1, 4, 4, 2, 1]$ and randomly sample the remaining ones from $\text{UniformChoice}([1, 2, 2])$. For α , which mainly controls the instrument strength, we use a deterministic value to guarantee valid instruments:

$$\alpha_{ij} \begin{cases} 0, & \text{for } i \neq j \text{ and } i, j > 8, \\ 1, & \text{for } i \neq j \leq 8 \end{cases} \quad (24)$$

We set the dispersion to $\theta = 2$ and the zero probability value $\eta = [0, \dots, 0, 0.8, \dots, 0.8]$. For the confounding composition Ω_C , we fix the first components to $[0.2, 0.3, 0.2, 0.1]$, to ensure that the most dominating parts of the composition are also more strongly influenced by confounding. Then we sample the remaining components of Ω_C from $\text{UniformChoice}([0.01, 0.05])$ and eventually apply the closure operator C to ensure Ω_C is a composition. For the second stage, we fix ground truth parameters $\beta_0 = 1, \beta_{\log} = [-10, -5, -5, -5, 10, 5, 5, 5, 0, \dots, 0]$, which results in $\beta = V^T \beta_{\log}$ and the confounding parameter $c_Y = [10, 10, 5, 15, -5, -5, -5, -5, -5, -5, -5, 0, \dots, 0]$.

For a brief overview, we visualize the first five components of the $\text{ilr}(X)$ coordinates versus the observed Y and the true causal effect in Figure S14 and show barplots of the generated data in Figure S13.

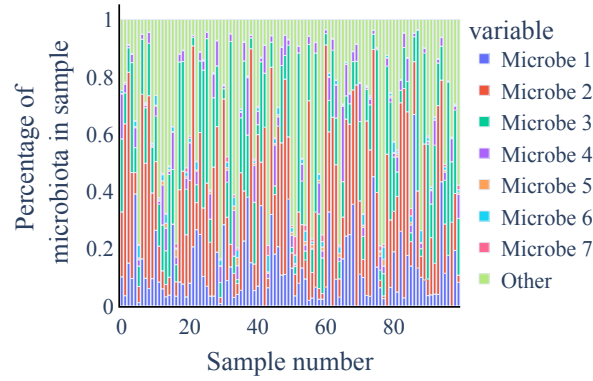


Figure S15. Setting B with $p = 250, q = 10$: The barplot shows the different compositions of the first 100 samples in the dataset. We still observe a few dominating components and many small components with an overall high variability.

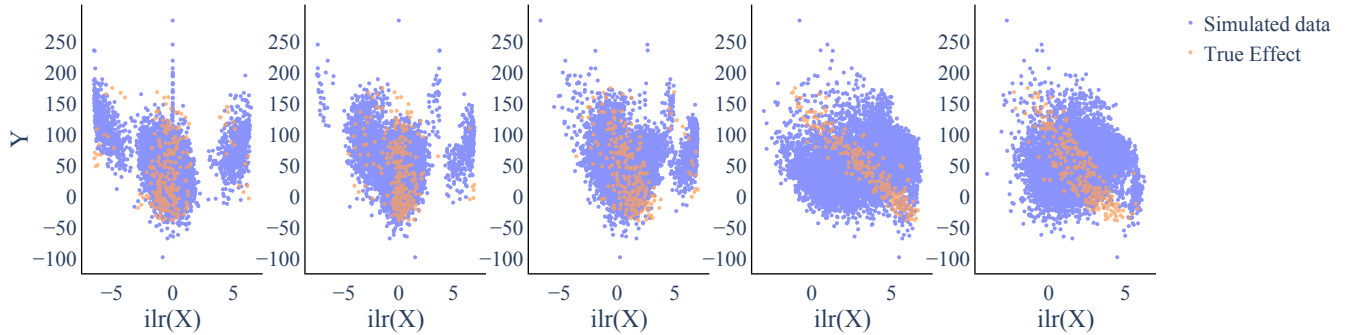


Figure S16. Setting B with $p = 250, q = 10$: Each plot shows one of the first five components of $\text{ilr}(X) \in \mathbb{R}^{249}$ vs. the confounded outcome (blue) and the true effect (orange). The dataset shows strong confounding in some of the components as the true effect and the observed effect actually contradict each other. We expect the two-stage methods to perform better than the naive regression in such scenarios. We can thus check if the two-stage methods are still able to make use of the instrument Z despite the misspecified first stage.

Setting B with $p = 250, q = 10$

We consider now the second high-dimensional scenario for Setting B with $p = 250$. The parameters for Setting B with $p = 250$ are very close to the parameters for Setting B with $p = 30$.

Again, we consider the following generative model based on Equation (23). We fix $Z_{\min} = 0, Z_{\max} = 10, U_{\min} = 0.2, U_{\max} = 3$. To ensure a handful of components dominating the composition, we fix the first 8 entries of α_0 to be $[1, 1, 2, 1, 4, 4, 2, 1, 4, 4, 2, 1]$ and randomly sample the remaining ones from $\text{UniformChoice}([1, 2, 2])$. For α , which mainly controls the instrument strength, we use a deterministic value to guarantee valid instruments:

$$\alpha_{ij} \begin{cases} 0, & \text{for } i \neq j \text{ and } i, j > 8, \\ 1, & \text{for } i \neq j \leq 8 \end{cases} \quad (25)$$

We set the dispersion to $\theta = 2$ and the zero probability value $\eta = [0, \dots, 0, 0.8, \dots, 0.8]$. For the confounding composition Ω_C , we fix the first components to $[0.2, 0.3, 0.2, 0.1]$, to ensure that the most dominating parts of the composition are also more strongly influenced by confounding. Then we sample the remaining components of Ω_C from $\text{UniformChoice}([0.01, 0.05])$ and eventually apply the closure operator C to ensure Ω_C is a composition. For the second stage, we fix ground truth parameters $\beta_0 = 1, \beta_{\log} = [-10, -5, -5, -5, 10, 5, 5, 5, 0, \dots, 0]$, which results in $\beta = V^T \beta_{\log}$ and the confounding parameter $c_Y = [10, 10, 5, 15, -5, -5, -5, -5, -5, -5, -5, 0, \dots, 0]$.

For a brief overview, we visualize the first five components of the $\text{ilr}(X)$ coordinates versus the observed Y and the true causal effect in Figure S16 and show barplots of the generated data in Figure S15.

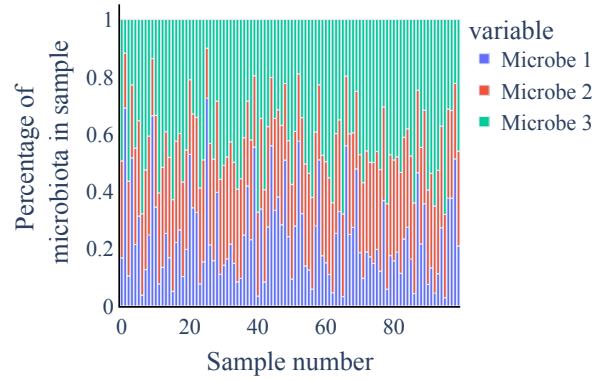


Figure S17. Setting A with $q = 2, p = 3$ and weak instruments: The barplot shows the different composition in each sample (plotted here for the first 100 samples). Microbe 2 has a relatively small value whereas microbe 1 and microbe 3 dominate the composition by high variation.

Further Settings for Robustness Evaluation

By assuming a misspecified first stage in Setting B via the ZINegBinom distribution, we already started to evaluate the robustness of our methods. Nevertheless, we will further relax different requirements within Setting A. We evaluate the robustness via two additional scenarios

1. We relax the assumption of a valid instrument and test the sensitivity of the methods with respect to weak instruments.
2. We assume a non-linear ground truth relationship f for the second stage, a scenario for which all the considered models are misspecified.

Weak Instrument

“Strong instruments” resp. “valid instruments” are a prerequisite for successful two-stage estimation and one of the key discussion points in applications of two-stage instrumental variable estimation. Instrument strength for $p = 1$ is typically measured via the first-stage F-statistic with a value > 10 being considered sufficient to avoid weak instrument bias in 2SLS [72]. For $p > 1$, measuring instrument strength is not as straightforward [73] and we thus report F-statistics for each dimension of the treatment (either $X \in \mathbb{S}^{p-1}$ or $\text{ilr}(X) \in \mathbb{R}^{p-1}$) separately. Theoretically, the estimation bias can become arbitrarily large (even in the large data limit) for weak instruments. To quantitatively assess the effect of weak instruments in our specific applications, we provide an additional simulation scenario and its results (see Supplementary Material S8) for a weak instrument settings.

Setting A with $p = 3, q = 2$ and weak instruments For testing in a weak instrument setting, we return to Setting A. We mostly control the instrument strength via α and use higher or lower α values to obtain a strong or weak instrument setting. We choose the following parameters for a weak instrument:

$$\mu_c = -2, \alpha_0 = [4, 1], \alpha = \begin{bmatrix} 0.05 & 0.01 \\ 0.2 & 0 \end{bmatrix}, c_X = [1, 1], \beta_0 = 2, \beta = [6, 2], c_Y = 4 \quad (26)$$

The first stage F-test for the two components of $\text{ilr}(X)$ gives (6.9, 4.7), much weaker than the previous settings. Again we show a barplot (Figure S17) and a ternary plot (Figure S18) of the generated data. The observed data as well as the true causal effect are shown in Figure S19.

Nonlinear Second Stage

Contrary to the previous scenarios, we now consider a non-linear f , resulting in a misspecified second stage for most of our methods. Note that in this scenario all two-stage methods as well as the naive regression will be misspecified in the second stage.

Setting A with $p = 3, q = 2$ and non-linear f Specifically, we replace the linear function for Y in Equation (21) with

$$Y = \beta_0 + \frac{1}{100} \mathbf{1}^T (\text{ilr}(X) + 1)^3 + 10 \cdot \mathbf{1}^T \sin(\text{ilr}(X)) + c_Y U. \quad (27)$$

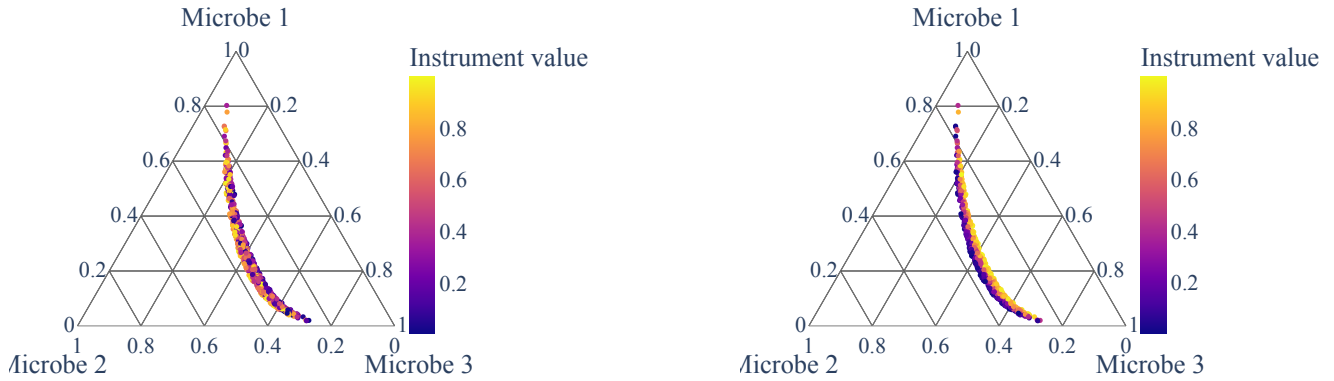


Figure S18. Setting A with $q = 2, p = 3$ and weak instruments: The ternary plots are colored by first (left) and second (right) instrument. The composition of the instrument is barely influenced by the value of Z .

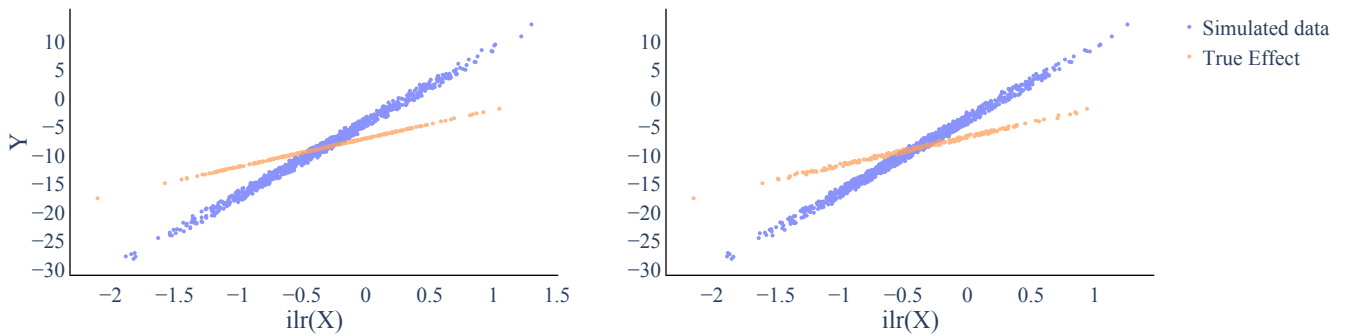


Figure S19. Setting A with $q = 2, p = 3$ and weak instruments: Both plots show one component of $\text{ilr}(X) \in \mathbb{R}^2$ vs. the confounded outcome (blue) and the true effect (orange). Due to the confounding, both effects do not overlap. As we are in the weaker instrument setting, we expect the methods to perform not as stable as in the previous cases where we had a stronger instrument available.

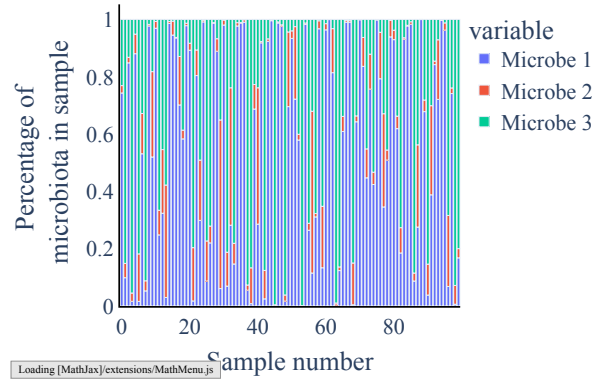


Figure S20. Setting A with $p = 3, q = 2$ and a non-linear function form of f : The barplot shows the different composition for each sample (for the 100 first data points). Microbe 1 and 2 dominate the composition with high variance.

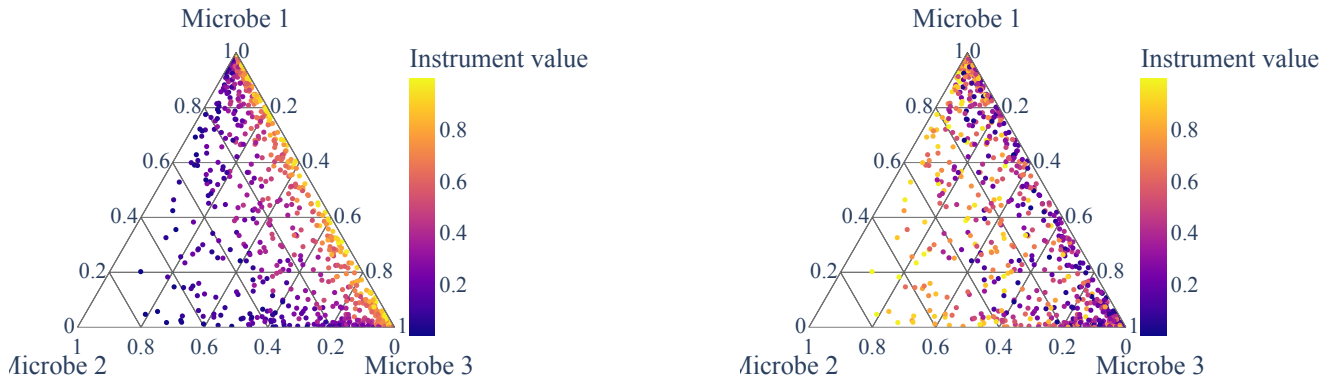


Figure S21. Setting A with $p = 3, q = 2$ and a non-linear function form of f : The ternary plots for the non-linear setup with $q = 2$, colored by first (left) and second (right) instrument. Note that the first stage is still linear in $\text{ilr}(X)$. Thus, the generation of the X values is not affected by the change in f .

The remaining parameters are chosen to yield a strong instrument, ensuring that any performance differences are not (in addition) due to weak instrument bias:

$$\mu_c = -1, \alpha_0 = [1, 1], \alpha = \begin{bmatrix} 4 & 1 \\ -1 & 3 \end{bmatrix}, c_X = [2, 2] \beta_0 = 5, \beta = [6, 2], c_Y = 4 \quad (28)$$

Note that in this setting β cannot be interpreted directly as the causal parameters, since the true causal effect also has a non-linear dependence on $\text{ilr}(X)$. Since the first stage remains unchanged, we can still use an F-test to assess instrument strength, which results in $(164.7, 76.4)$, a solid indicator for a strong instrument. Again we show a barplot (Figure S20) and a ternary plot (Figure S21) of the generated data. The observed data as well as the true causal effect are shown in Figure S22.

Scarce Data Example $p \gg n$

We return to Setting A with linear dependencies in both stages. However, in the scenarios before, we assumed a large dataset ($n = 10,000$) for the methods to work on. In many real applications, this might not be the case. Thus we choose to include an additional robustness aspect concentrating on the scenario $p \gg n$. In this particular case we chose $p = 250$ and $n = 100$.

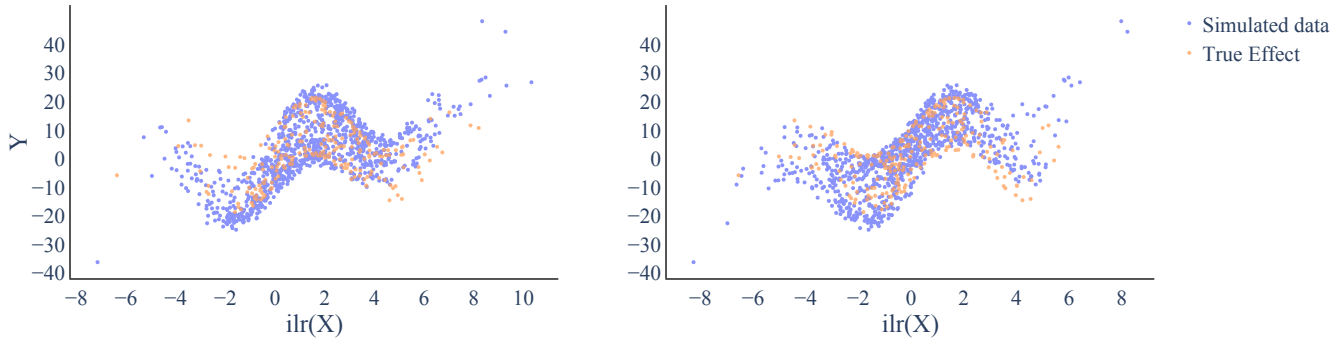


Figure S22. Setting A with $p = 3, q = 2$ and a non-linear function form of f : Both plots show one component of $\text{ilr}(X) \in \mathbb{R}^2$ vs. the confounded outcome (blue) and the true effect (orange). The effect both of the confounded outcome and the true effect show a non-linear dependency towards the individual $\text{ilr}(X)$ components.

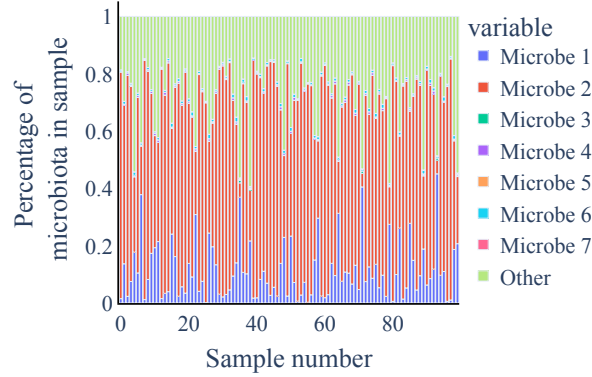


Figure S23. Setting A with $n = 100, p = 250, q = 10$: The barplot shows the composition of the 100 samples. The compositions are dominated by a few species.

Setting A with $p = 250, q = 10$ and $n = 100$ The choice of parameter is the same to Setting A with $n = 10,000$, however we only include the first 100 samples for the estimation:

$$\mu_c = 3, \alpha_0 = [1, 1, 3, 1, 1, 1, 3, 1, 1, 1, 3, 1, 0, \dots, 0], \alpha_{ij} \begin{cases} 0, & \text{for } i \neq j \text{ and } i, j > 8, \\ 1, & \text{for } i \neq j \leq 8 \end{cases},$$

$$c_X = [-1, 2, -1, 2, -1, 2, -2, 1, -2, 1, -2, 1, 0, \dots, 0], \beta_0 = 5, \beta_{\log} = [10, 5, 5, 5, -10, -5, -5, -5, 0, \dots, 0],$$

$$\beta = V^T \cdot \beta_{\log}, c_Y = 5$$

for $i \in \{1, \dots, p-1\}, j \in \{1, \dots, q\}$ and V providing the orthonormal basis for the ilr -transformation (see Supplementary Material S2).

For the sake of completeness, we show a barplot (Figure S23) of the generated data. We note that the samples are the first 100 samples of the larger dataset of the original Setting A with $p = 250, q = 10$ and $n = 10,000$. The observed data as well as the true causal effect are shown in Figure S24.

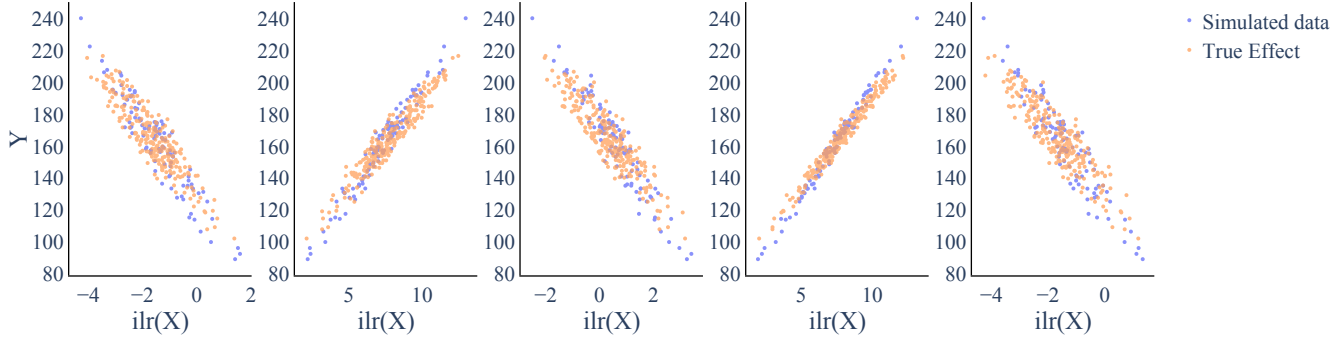


Figure S24. Setting A with $n = 100$, $p = 250$, $q = 10$: Both plots show one component of $\text{ilr}(X) \in \mathbb{R}^{249}$ vs. the confounded outcome (blue) and the true effect (orange). Due to the confounding, the observed and the causal effect do not overlap. However, we expect the instrument Z to factor out the confounding effect and enable the two-stage methods to identify the causal effect. Note that now we consider a sample size of $n = 100$.

S7 Method Training

Dirichlet Regression

The mean of the Dirichlet distribution is given by $\mu_{\text{Diri}} = \frac{\alpha_j}{\sum_{j=1}^p \alpha_j}$. Here, we consider the following model for the mean components

$$\mathbb{E}[X_{ij}] = \frac{\alpha_j}{\sum_{j=1}^p \alpha_j} = \frac{\alpha_j(Z_i)}{\sum_{j=1}^p \alpha_j(Z_i)} \quad (29)$$

$$\log(\alpha_j(Z_i)) = \omega_{0j} + \omega_j Z_j. \quad (30)$$

The maximum likelihood function is then given by

$$l(\alpha; X, Z) = \frac{1}{n} \sum_{i=1}^n \log \Gamma \left(\sum_{j=1}^p \exp\{\omega_{0j} + \omega_j Z_i\} \right) \quad (31)$$

$$+ \frac{1}{n} \sum_{i=1}^n \sum_{j=1}^p \left(\log(X_{ij}) \left(\exp\{\omega_{0j} + \omega_j Z_i\} - 1 \right) - \log \Gamma \left(\exp\{\omega_{0j} + \omega_j Z_i\} \right) \right). \quad (32)$$

Additionally, we introduce a sparsity enforcing regularization term to arrive at the following objective function

$$\min_{\omega} -l(\alpha; X, Z) + \lambda_{\text{dirichlet}} \sum_{j=1}^p |\omega_j| \quad (33)$$

with $\lambda_{\text{dirichlet}} \geq 0$. For each Dirichlet regression, we pick $\lambda_{\text{dirichlet}}$ from the set $\{0.1, 1, 2, 5, 10\}$ by model selection via the Bayesian Information Criterion ($BIC = q \cdot \log(n) - 2 \cdot (\hat{L})$, with \hat{L} being the likelihood value). We train the model for each available λ value in the set and choose the model with minimal BIC. For the starting point α_{start} we fit a Dirichlet distribution on those X for which all $|Z| < 0.2$ by maximum likelihood estimation.

Log-contrast Regression

The log-contrast regression is enforcing sparsity via an ℓ_1 penalty on the β parameters.

$$\min_{\beta} \sum_{i=1}^n \mathcal{L}(x_i, y_i, \beta) + \lambda \|\beta\|_1 \quad \text{s.t.} \quad \sum_{i=1}^p \beta_i = 0. \quad (34)$$

This estimation respects the compositional nature of x while retaining the association between the entry β_i and the relative abundance of the individual component x_i .

In our examples, we focus mainly on continuous $y \in \mathbb{R}$ and the squared loss $\mathcal{L}(x, y, \beta) = (y - \beta^T \log(x))^2$. However, the framework also supports different loss functions.

For robust Lasso regression, the Huber loss can be applied.

$$\mathcal{L}(x_i, y_i, \beta) = \mathcal{H}_\delta(x_i, y_i, \beta) = \begin{cases} \frac{1}{2}(y_i - \beta^T \log(x_i))^2 & \text{for } |y_i - \beta^T \log(x_i)| < \delta \\ \delta(|y_i - \beta^T \log(x_i)| - \frac{1}{2}\delta), & \text{otherwise.} \end{cases} \quad (35)$$

The Huber Loss combines the squared loss and the absolute loss. It is less sensitive to outliers than the squared loss, but remains differentiable at 0 in contrast to the absolute loss.

Moreover, for classification tasks with $y_i \in \{-1, 1\}$, we can directly use the squared Hinge loss for \mathcal{L} with:

$$\mathcal{L}(x_i, y_i, \beta) = l(x_i, y_i, \beta) \text{ with } l(x_i, y_i, \beta) = \begin{cases} (1 - (y_i \beta^T \log(x_i)))^2, & \text{if } y_i \beta^T \log(x_i) \leq 1 \\ 0, & \text{if } y_i \beta^T \log(x_i) > 1 \end{cases} \quad (36)$$

or a ‘‘Huberized’’ version thereof:

$$\mathcal{L}(x_i, y_i, \beta) = l_\delta(x_i, y_i, \beta) \text{ with } l_\delta(x_i, y_i, \beta) = \begin{cases} (1 - (y_i \beta^T \log(x_i)))^2, & \text{if } \delta \leq y_i \beta^T \log(x_i) \leq 1 \\ (1 - \delta)(1 + \delta - 2y_i \beta^T \log(x_i)), & \text{if } y_i \beta^T \log(x_i) \leq \delta \\ 0, & \text{if } y_i \beta^T \log(x_i) > 1 \end{cases} \quad (37)$$

We refer to [89] for further loss functions and a more detailed overview.

We now continue with the description of the setup used in the following result section. The results on the synthetic data and the real data in Supplementary Material S8 are based on the squared loss:

$$\min_{\beta} \sum_{i=1}^n \|y_i - \beta^T \log(x_i)\|_2^2 + \lambda \|\beta\|_1 \quad \text{subject to } \sum_{i=1}^p \beta_i = 0. \quad (38)$$

Furthermore, for the real data we also show the results for a binary outcome $y_i \in \{-1, 1\}$ based on the squared Hinge loss (Equation (36)).

We solve the underlying optimization problems with the c-lasso package, a Python package for constrained sparse regression [89]. The c-lasso packages comprises several model selection schemes, including a theoretically-derived λ_0 parameter, k-fold cross-validation, and stability selection.

Here, we consider stability selection for tuning λ . The method comprises the hyperparameter $t_{\text{threshold}}$ which determines the number of coefficients included in the final model. In our training, we set the same $t_{\text{threshold}}$ for the naive regression as well as the two-stage methods to have a fair comparison. In all our training scenarios with generated data we find $t_{\text{threshold}} = 0.7$ to be a reasonable default value. For the real data scenario we found $t_{\text{threshold}} = 0.65$ to be more sensible.

We use Setting B with $p = 30$ and $q = 10$ as a representative example to illustrate the impact of the threshold value. Figure S25 shows the stability profile of the β coefficients and their attributed probability of entering the model. The threshold value $t_{\text{threshold}} = 0.7$ works as a cut off for the relevant coefficients. The upper panel shows the results for the naive regression, whereas the lower panel shows the results for the ILR+LC regression (working on the exact same data).

Moreover, the method also returns the coefficient values across the λ -path, i.e., the entry of coefficients into the model for the corresponding λ (see Figure S26). Further improvements may be achieved by taking the path and individual analysis into account instead of proposing a general $t_{\text{threshold}}$, however, this simple yet effective approach was sufficient for our purposes in this work.

S8 Method Results

For the comparison of the different methods, we make use of three approaches:

1. $\hat{\beta}$ -MSE: As long as the second stage is wellspecified and linear, we can compare the estimated causal parameters $\hat{\beta}$ for the various approaches (where applicable).
2. FZ/FNZ: As long as the second stage is wellspecified and linear, we can additionally compare the number of false zero values and false non-zero values to quantify support recovery.
3. OOS MSE: In the general case, the causal performance measure is measured by an ‘‘out of sample error’’ (OOS MSE) which denotes the mean squared error between the true value of Y under an intervention $do(X = x)$ and the predicted causal effect $\mathbb{E}[Y | do(X)]$ of our model, given by $\hat{f}(x)$. For the interventional X , we simulate 250 additional compositional data points according to the underlying model, but using a different seed and thus disconnecting them from the instrument Z and the confounder U . Thus, we receive a true interventional X which still preserves data characteristics.

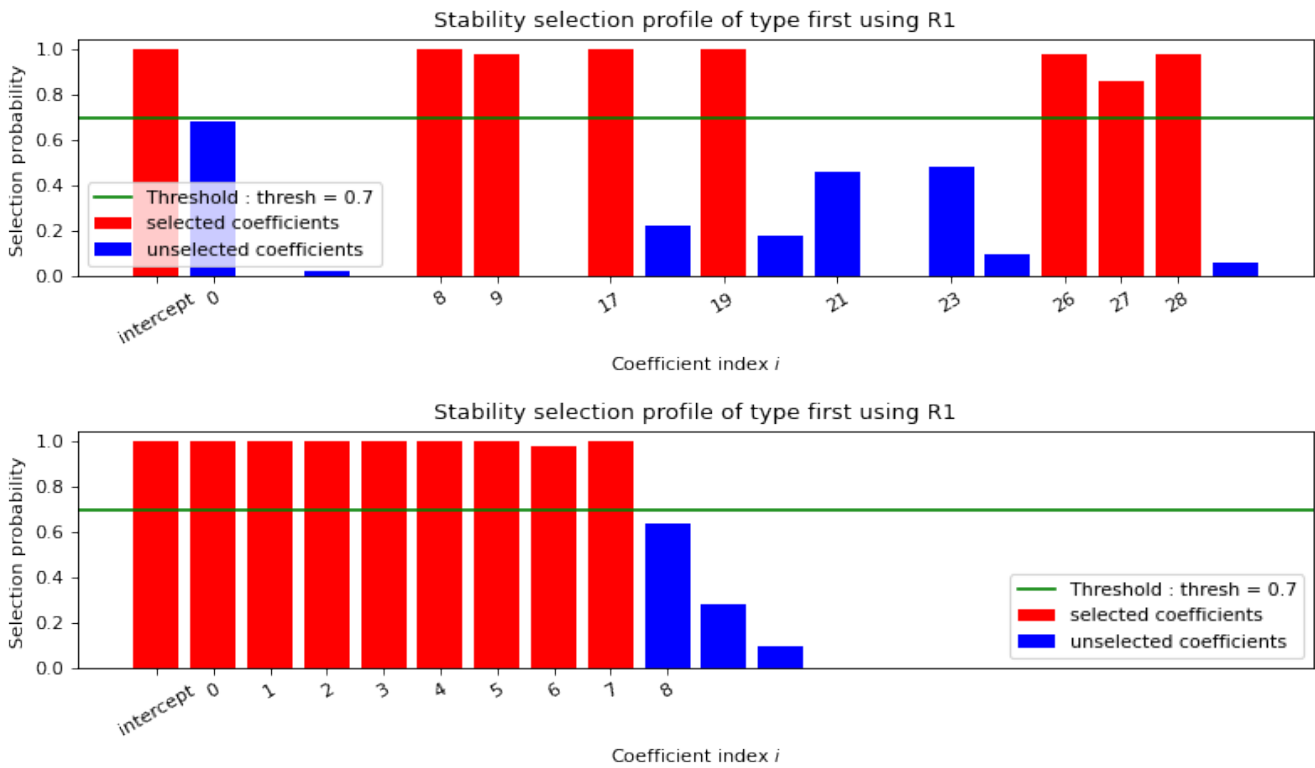


Figure S25. Stability profiles for sparse log contrast regression with c-lasso: The barplots show the model selection probability of the β coefficients. The upper panel shows the example for the naive regression. The lower panel shows the results for the same setting for ILR+LC regression. Both models are fairly certain about the main drivers.

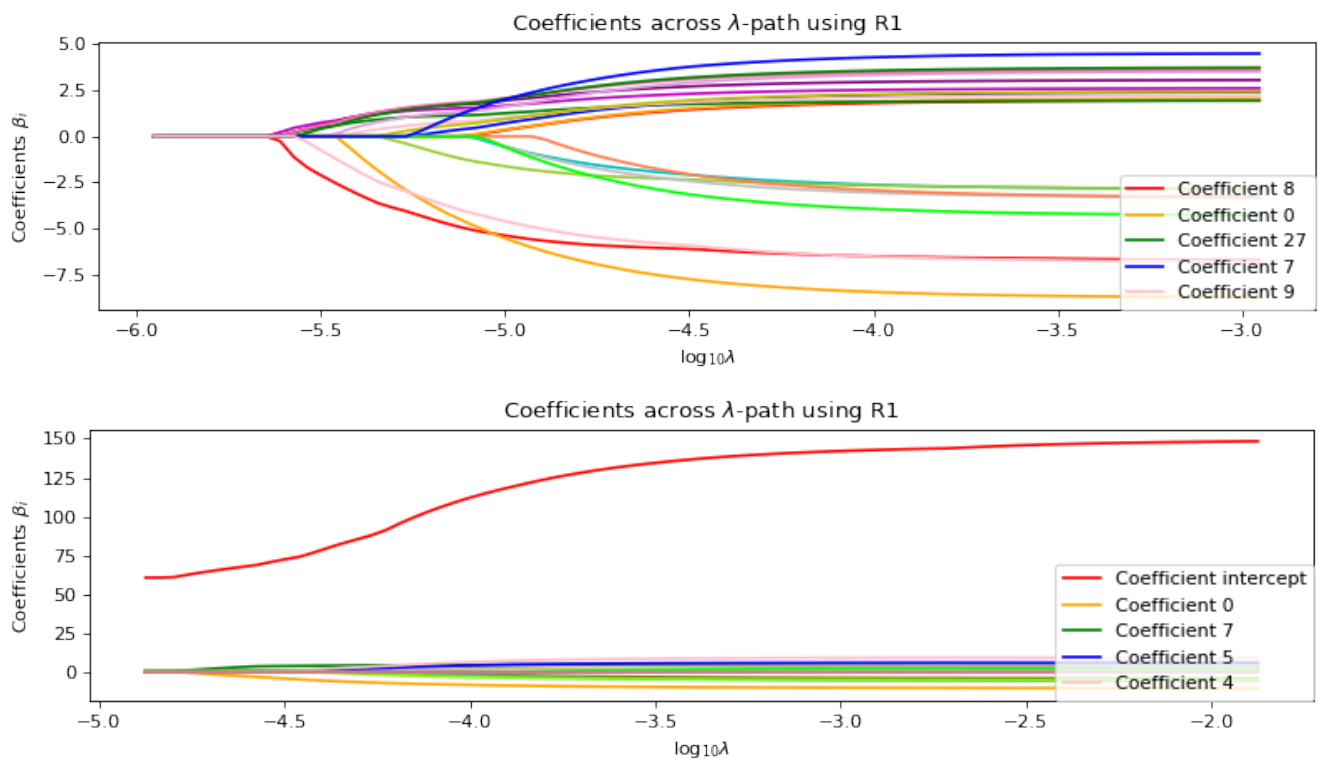


Figure S26. Corresponding λ -path for β coefficients: The plots show the individual coefficients for the different λ values. The upper plot shows the β coefficients for the naive regression, the lower plot presents the coefficients for the two-stage method ILR+LC.

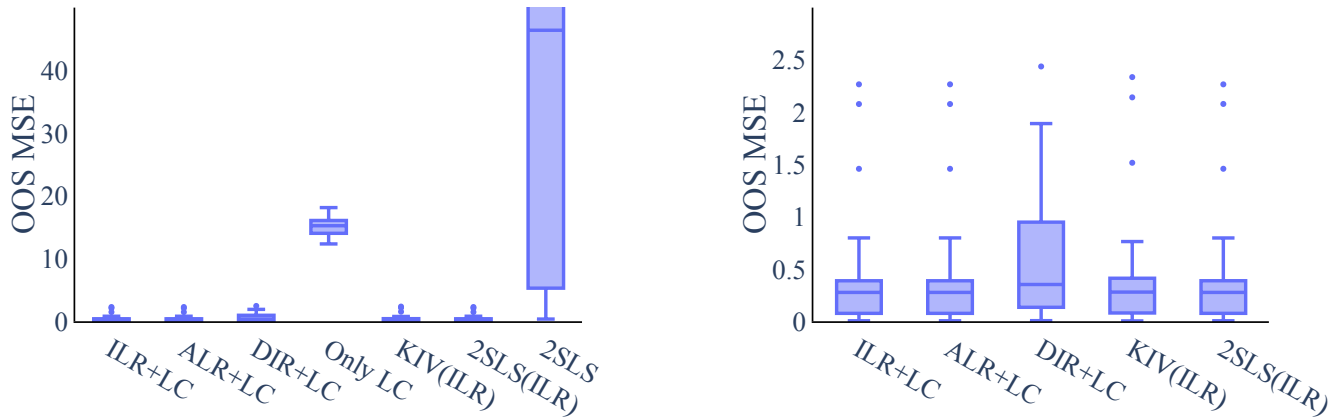


Figure S27. Setting A with $p = 3, q = 2$: The boxplots show the OOS MSE of 50 runs. The naive regression Only LC and 2SLS (left) perform way worse compared to the other approaches. When we adjust the y-scale (right), DIR+LC also shows a higher OOS MSE than ILR+LC etc. DIR+LC possibly suffers from the misspecified first stage. Note that ALR+LC, ILR+LC, 2SLS_{ILR} are equivalent in the low-dimensional case.

For each data generating setup, we provide confidence intervals for the methods' results by performing the data generation and the method evaluation 50 times on different random seeds. In each run, we sample $n = 1000$ datapoints in the $p = 3$ scenario and 10,000 datapoints in the $p = 30$ and $p = 250$ scenario. We compute the OOS MSE as well as the $\hat{\beta}$ -MSE and FZ/FNZ (if applicable). Some of the figures in this section are extended or more complete versions of the numbers given in the table in the main body (see Tables 1 and 2), where some less relevant results have been omitted for readability.

Setting A

Setting A with $p = 3, q = 2$

This setting is a wellspecified setting for ALR+LC, 2SLS_{ILR} and ILR+LC. Moreover, confounding is present (see Figure S5) which additionally gives us reason to expect a much better performance of the two-stage methods than the naive regression $X \rightarrow Y$ in terms of OOS MSE. The results in Figure S27, largely verify this expectation. The naive regression has a clear disadvantage due to confounding and picks up on spurious correlations as an effect coming from X . Two-stage methods work well when relying on a strong instrument, helping the methods to factor out the confounding and identifying the true causal effect. Figure S28 shows the causal parameter estimates $\hat{\beta}$ and further corroborates our claims that two-stage methods significantly outperform naive regression. The effects found via naive regression overestimate the direct causal effect strength from X , whereas all two-stage methods recover the true causal parameters β well. Only DIR+LC suffers slightly from the misspecified first stage compared to the other wellspecified two-stage approaches. It is noteworthy that DIR+LC works reasonably well despite our manual two-stage procedure with a “forbidden” non-linear regression in the first stage. Since we are in the low-dimensional setting with no sparsity regularization, the results of ILR+LC, ALR+LC and 2SLS_{ILR} are equivalent.

Setting A with $p = 30, q = 10$

Microbiome compositional data is typically high-dimensional and comprises many zero values. Moreover, it is often assumed that only a few microbial compositions (and hence β parameters) influence an outcome of interest Y . Thus, in the following, we aim to be close to such a scenario by assuming a sparse β as ground truth and by simulating X with a few dominating compositions in the data generating process (see Supplementary Material S6).

Note that for higher-dimensional approaches, we omit results for DIR+LC due to computational issues stemming from the maximum likelihood estimation of the α_0 and α parameters in the first stage. 2SLS, which ignores the compositionality of X altogether, is not able to converge at all.

For higher dimensions, the lack of regularization in the ILR methods becomes obvious (Figure S29), both for 2SLS_{ILR} and KIV_{ILR}. The methods become more volatile and 2SLS_{ILR} is unable to detect any zero values in β (see Figure S30). On the other hand, the naive regression is able to identify zero β s correctly, but suffers from confounding and thus over- or underestimates the true influential β s. Only the regularized two-stage approaches are able to recover the true causal β s, both the influential coefficients as well as the zero values.

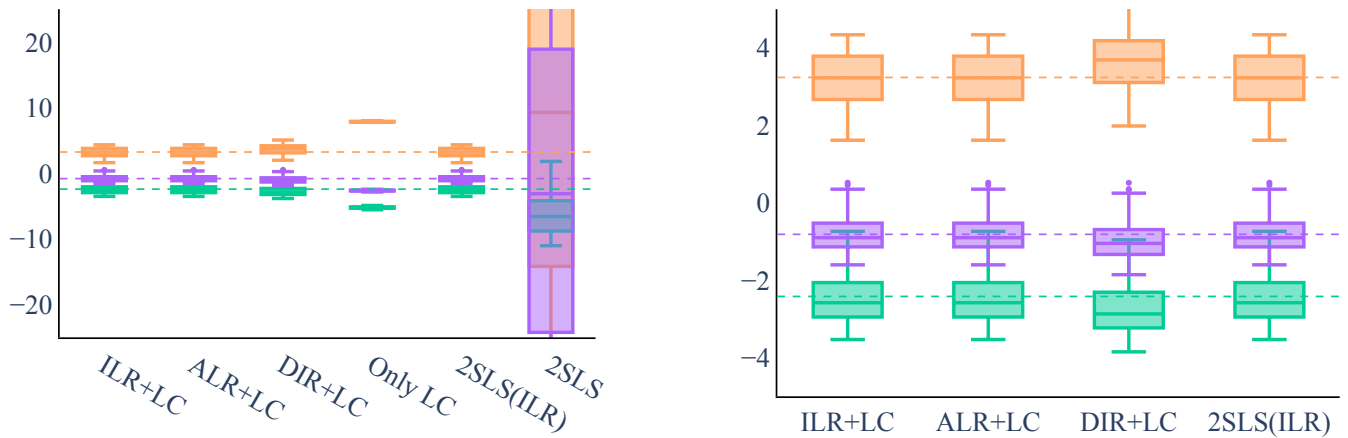


Figure S28. Setting A with $p = 3, q = 2$: The boxplots show the $\hat{\beta}$ values for the 50 runs for each of the 3 β coefficients (dashed lines). The two-stage methods, except 2SLS, are able to recover the causal effect on average. The naive regression method overestimates the effect. Moreover, it does so with a high degree of confidence as there is barely any variation in the $\hat{\beta}$ estimates (left). When we adjust the y-scale (right), DIR+LC shows a notable bias towards the solution of the naive regression (left). This might suggest that DIR+LC indeed suffers from the misspecified first stage and thus is not able to make use of the instrument Z as efficiently.

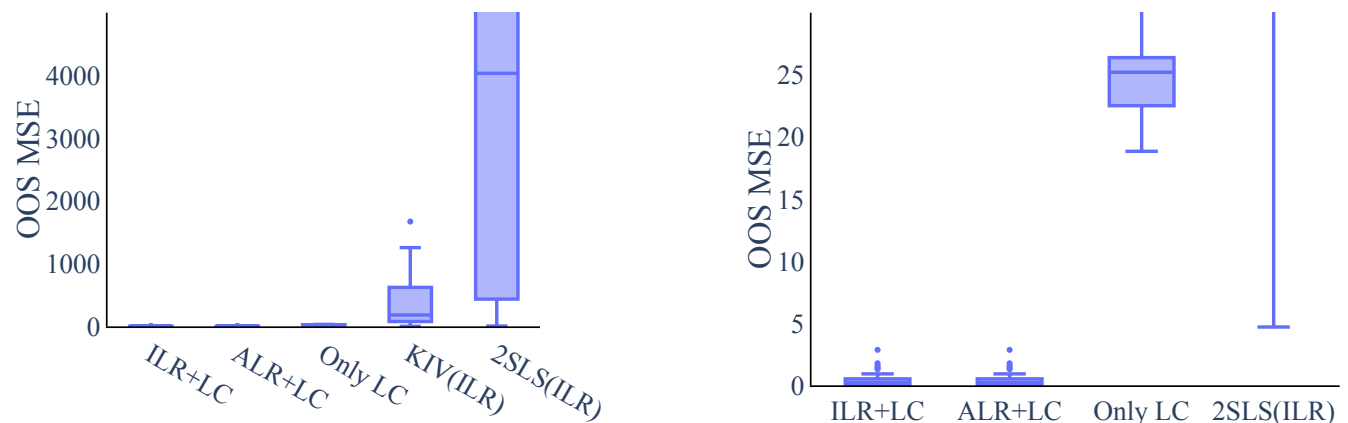


Figure S29. Setting A with $p = 30, q = 10$: The boxplots show the OOS MSE of 50 runs. 2SLS_{ILR} and KIV_{ILR} are volatile and lack sensible regularization (left). When we adjust the y-scale, we see that Only LC (right) performs also way worse compared to the regularized two-stage approaches.

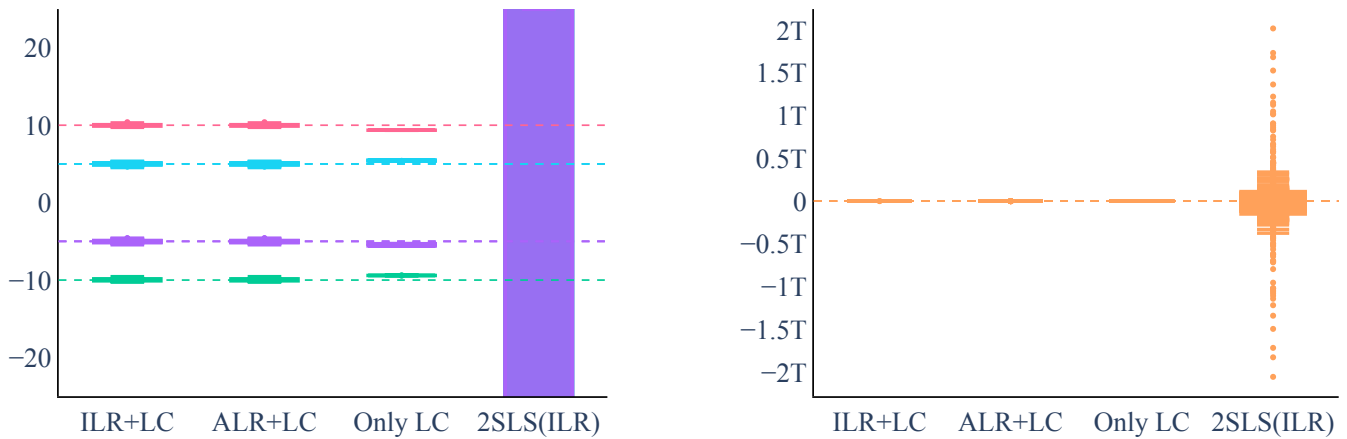


Figure S30. Setting A with $p = 30, q = 10$: The boxplots show the $\hat{\beta}$ values for the 50 runs for each of the 8 non-zero β coefficients (dashed lines, left) and the 22 zero β coefficients (dashed line, right). The two-stage methods are able to recover the causal effect on average, whereas the naive regression methods overestimate the effect (left). Moreover, Only LC does so with a high degree of confidence as there is barely any variation in the $\hat{\beta}$ estimates. $2SLS_{ILR}$ does not produce sensible estimates due to the missing regularization.

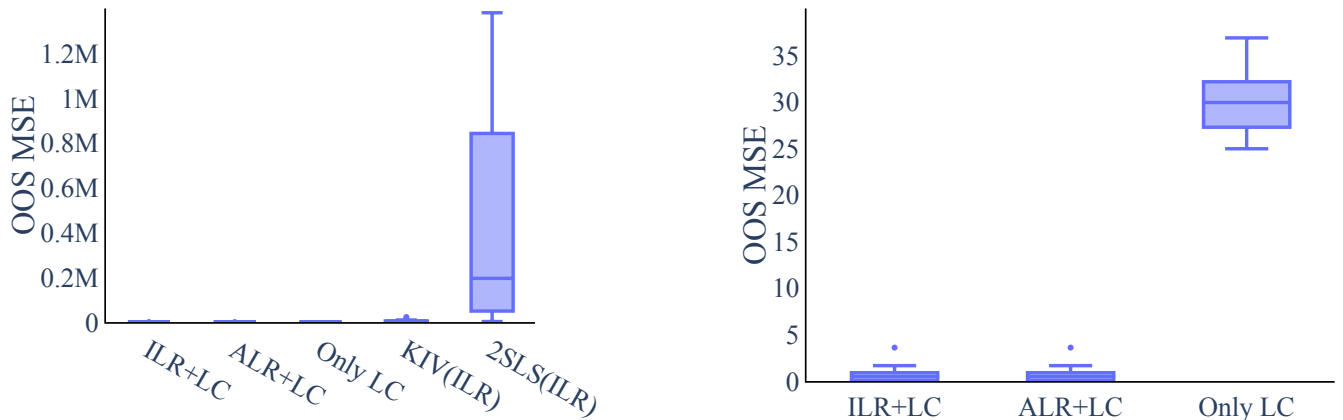


Figure S31. Setting A with $p = 250, q = 10$: The boxplots show the OOS MSE of 50 runs. $2SLS_{ILR}$ and KIV_{ILR} are volatile and lack sensible regularization (left). This problem is more pressing as the dimensionality grows. When we adjust the y-scale, we see that also Only LC (right) performs worse compared to the regularized two-stage approaches.

Setting A with $p = 250, q = 10$

To further test the approaches, we use another high-dimensional setup with $p = 250$. Again, we make use of the common assumption that only a few microbial compositions (and hence β parameters) influence an outcome of interest Y . We assume a sparse β as ground truth and run the models on X which has a few dominating species.

Note that for higher-dimensional approaches, we omit results for DIR+LC due to computational issues stemming from the maximum likelihood estimation of the α_0 and α parameters in the first stage. $2SLS$, which ignores the compositionality of X altogether, is not able to converge at all.

For $p = 250$, the problem of missing regularization in the ILR methods ($2SLS_{ILR}$ and KIV_{ILR}) becomes even more pronounced (Figure S31). For readability we thus omitted $2SLS_{ILR}$ from the β plots. Moreover, the naive regression is not even able to recover the full support, as it only identifies most, but not all, of the zero and non-zero β s correctly (see Figure S30). Only the regularized two-stage approaches are able to recover the true causal β s.

Setting B

In this part we will examine the methods for Setting B Equation (7). Note that the first stage is misspecified for the two-stage approaches, whereas the second stage is wellspecified for all methods.

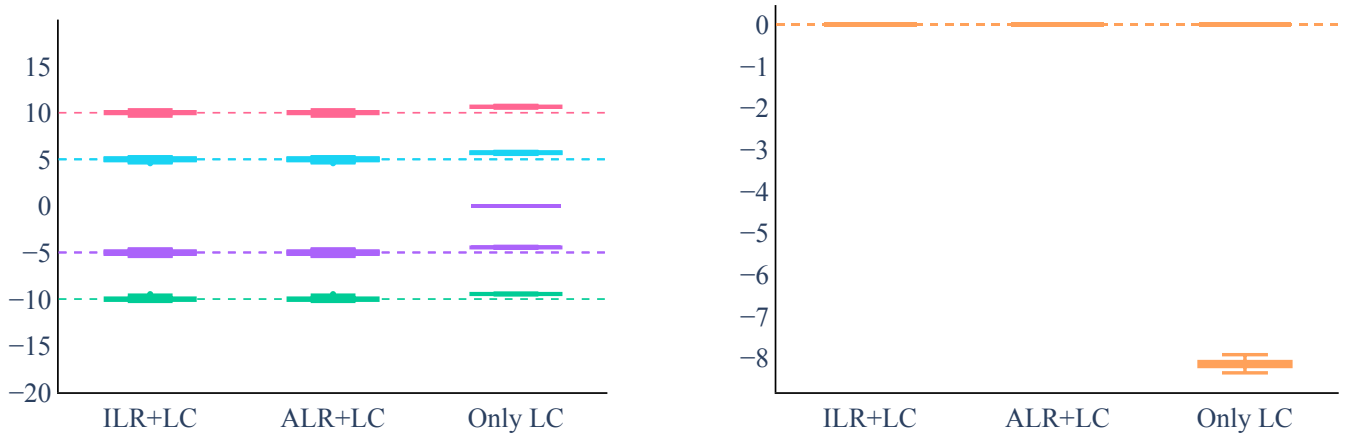


Figure S32. Setting A with $p = 250, q = 10$: The boxplots show the $\hat{\beta}$ values for the 50 runs for each of the 8 non-zero β coefficients (dashed lines, left) and the 242 zero β coefficients (dashed line, right). The two-stage methods are able to recover the causal effect on average, whereas the naive regression method is not able to recover the true support. 2SLS_{ILR} does not produce sensible estimates due to the missing regularization and is omitted for better readability.

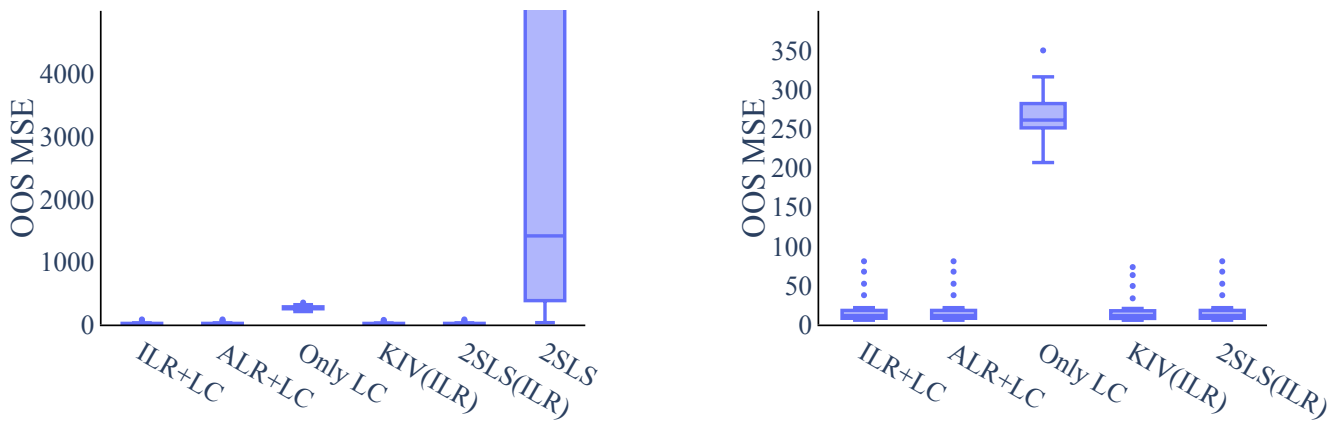


Figure S33. Setting B with $p = 3, q = 2$: The boxplots show the OOS MSE of 20 runs. 2SLS and DIR+LC perform way worse as compared to the two-stage approaches (left). When we adjust the y-scale (right), Only LC also cannot compare to the remaining two-stage approaches. ALR+LC, ILR+LC, 2SLS_{ILR} are equivalent in the low-dimensional case.

Setting B with $p = 3, q = 2$

Even in this low-dimensional scenario, DIR+LC suffers substantially from the misspecified second stage. It is not able to produce sensible estimates. We argue that this might be due to the “forbidden regression” issue. Furthermore, the naive regression is highly influenced by confounding. It even flips the estimated effect of two components, see Figure S34. Nevertheless the remaining two-stage methods, except 2SLS which ignores compositionality, perform reasonably well in recovering the true causal effect (see Figure S33).

Setting B with $p = 30, q = 10$

Microbiome compositional data is typically high-dimensional and comprises many zero values. Moreover, it is often assumed that only a few microbial compositions (and hence β parameters) influence an outcome of interest Y . Thus, in the following, we will emulate such a scenario and assume a sparse β as ground truth and additionally—as ZINegBinom can incorporate sparsity also on X —run the models on relatively sparse X (see Supplementary Material S6).

Note that for higher-dimensional approaches, we omit results for DIR+LC due to computational issues stemming from the maximum likelihood estimation of the α_0 and α parameters in the first stage.

Moreover, for $p = 30$, 2SLS_{ILR} already is unfit to capture the causal effect due to missing regularization. Due to its high OOS MSE value, we omitted 2SLS_{ILR} in Figure S36 for better readability. 2SLS, which ignores the compositionality of X altogether, is able to converge, but does not produce reasonable estimates.

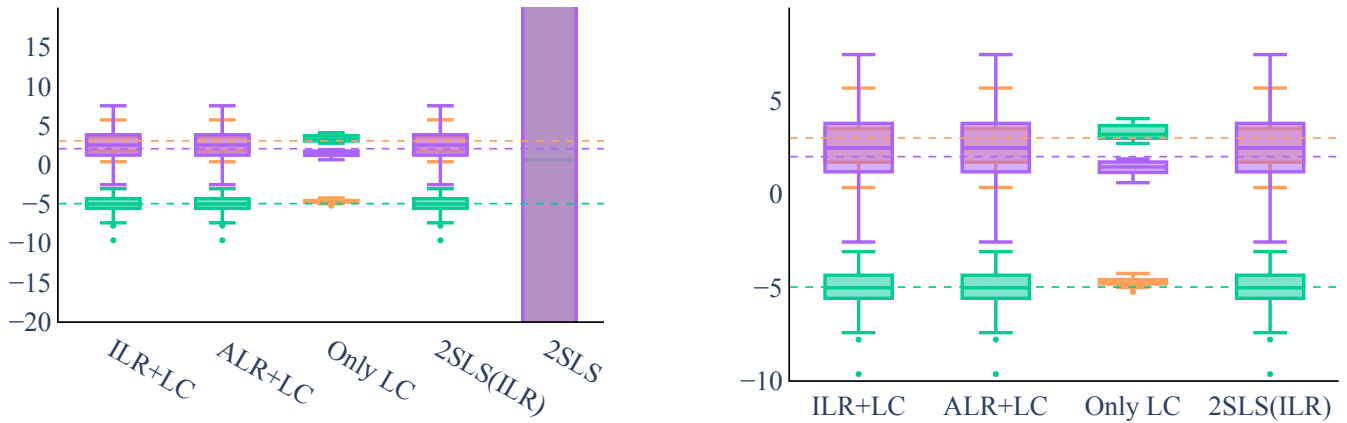


Figure S34. Setting B with $p = 3, q = 2$: The boxplots show the $\hat{\beta}$ values for the 20 runs for each of the 3 β coefficients. The two-stage methods (except for DIR+LC and 2SLS) are able to recover the true causal β s on average. However, when we adjust the y-scale (right), the problem of confounding becomes apparent: Only LC flips the sign of two of the non-zero β values.

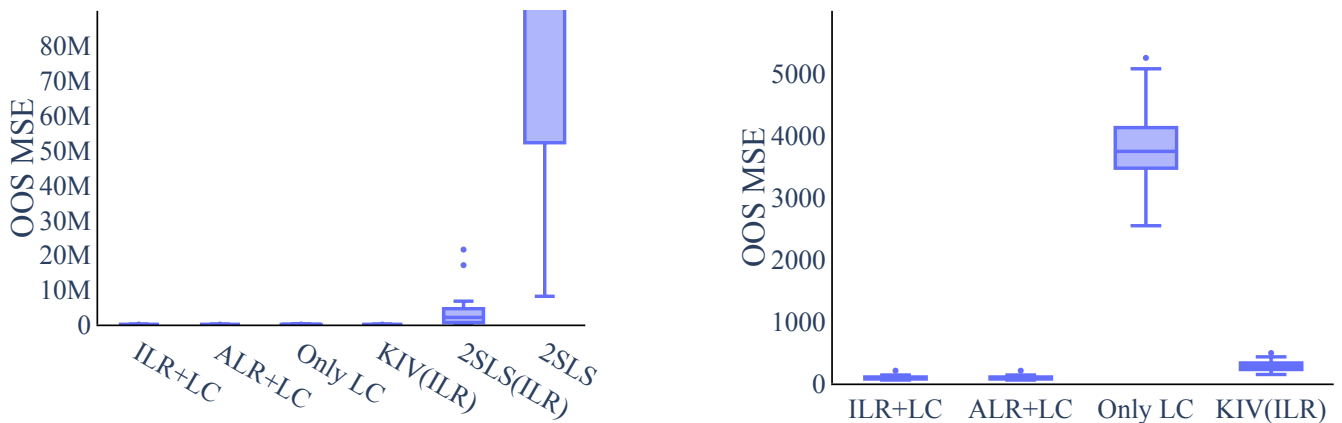


Figure S35. Setting B with $p = 30, q = 10$: The boxplots show the OOS MSE of 20 runs. $2SLS_{ILR}$ is only reasonable in low-dimensions (left). When we adjust the y-scale (right), we see that the remaining two-stage approaches outperform the naive regression.

For KIV_{ILR} , the difficulty of tuning the method in higher dimensions remains an issue (see Figure S35). The remaining two-stage approaches, however, benefit substantially from the instrumentation of X by Z . They outperform the naive regression both on OOS MSE (see Figure S35), as well as on the recovery of the true β values (see Figure S36). While the naive regression not only fails to recover the true β values, it also produces quite volatile estimates (see Figure S36).

Setting B with $p = 250, q = 10$

Microbiome compositional data is typically high-dimensional and comprises many zero values. Moreover, it is often assumed that only a few microbial compositions (and hence β parameters) influence an outcome of interest Y . Thus, in the following, we will emulate such a scenario and assume a sparse β as ground truth and additionally—as ZINegBinom can incorporate sparsity also on X —run the models on relatively sparse X (see Supplementary Material S6).

Note that for higher-dimensional approaches, we omit results for DIR+LC due to computational issues stemming from the maximum likelihood estimation of the α_0 and α parameters in the first stage.

Both high-dimensional scenarios generally agree in their outcomes; for $p = 250$ the shortcomings of the different approaches only get more enhanced.

While 2SLS, which ignores the compositionality of X altogether, is also able to converge for $p = 250$, it does not produce reasonable estimates. Further, the regularized two-stage methods still perform reasonably well, while $2SLS_{ILR}$ and KIV_{ILR} cannot match that performance (see Figure S37) due to the lack of sensible regularization. The naive approach can capture

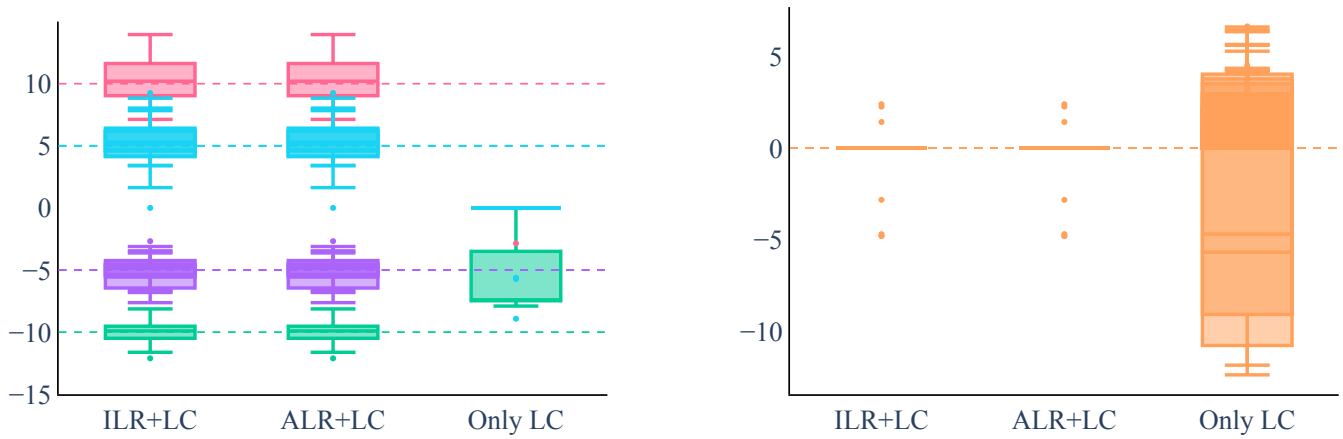


Figure S36. Setting B with $p = 30, q = 10$: The boxplots show the $\hat{\beta}$ values for the 20 runs for each of the 8 non-zero β coefficients (dashed lines, left) and the 22 zero β coefficients (dashed line, right). The naive regression Only LC is not able to recover the β values at all. ILR+LC and ALR+LC are better suited to recover the causal parameters when confounding is present. Despite the misspecified first stage, they are able to recover the causal β values on average.

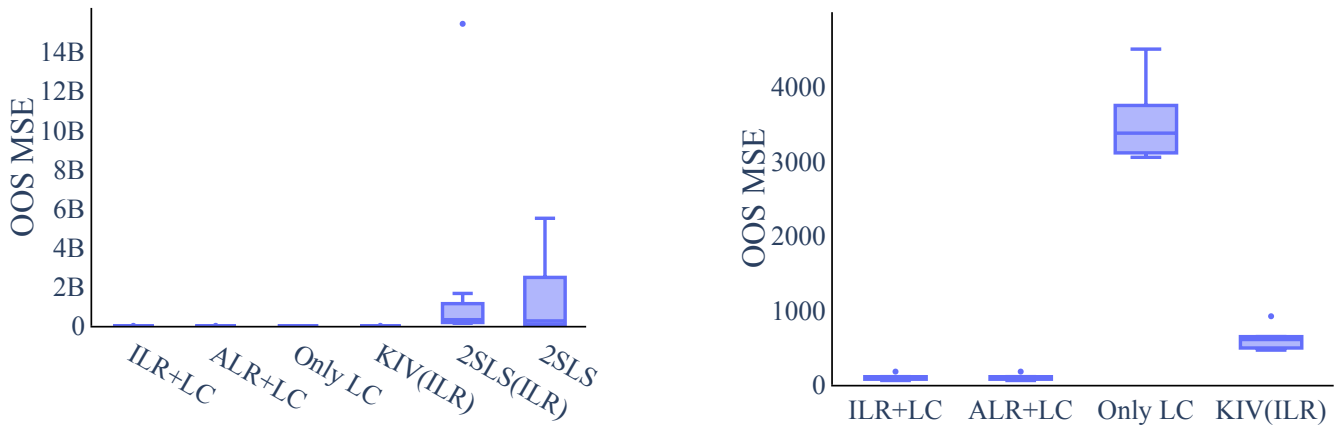


Figure S37. Setting B with $p = 250, q = 10$: The boxplots show the OOS MSE of 20 runs. $2SLS_{ILR}$ is only reasonable in low-dimensions and KIV_{ILR} is difficult to tune in higher dimensions (left). When we adjust the y-scale (right), we see that ILR+LC and ALR+LC outperform the naive regression.

neither the causal effect nor the causal β values (see Figures S37 and S38).

Further Settings for Robustness Estimation

We will analyze the results from our “robustness” scenarios including a weak instrument setting and a setting with a nonlinear functional relationship in the second stage.

Weak Instrument

Setting A with $p = 3, q = 2$ and weak instruments In a strong/valid instrument setting, two-stage methods have a clear advantage. To test the limitations of our methods, we now analyze an equivalent setting with a comparatively weak instrument. In this setting, confounding is still noticeable (see Figure S19) but the first stage F-statistic is much lower, indicating that we may suffer from weak instrument bias.

The two-stage methods have a higher variation in their estimates, both for OOS MSE and $\hat{\beta}$ (see Figures S39 and S40), whereas the naive regression does not change at all (since only the first stage data generation has changed). Nevertheless, the wellspecified two-stage methods (ALR+LC, ILR+LC, $2SLS_{ILR}$) still recover the causal effects better than the naive regression. Only the DIR+LC regression runs into problems due to two misspecified stages. We thus conclude that the “forbidden regression” is not necessarily detrimental to cause-effect estimation when the instrument is strong, but can indeed result in unreliable results for weaker instruments.

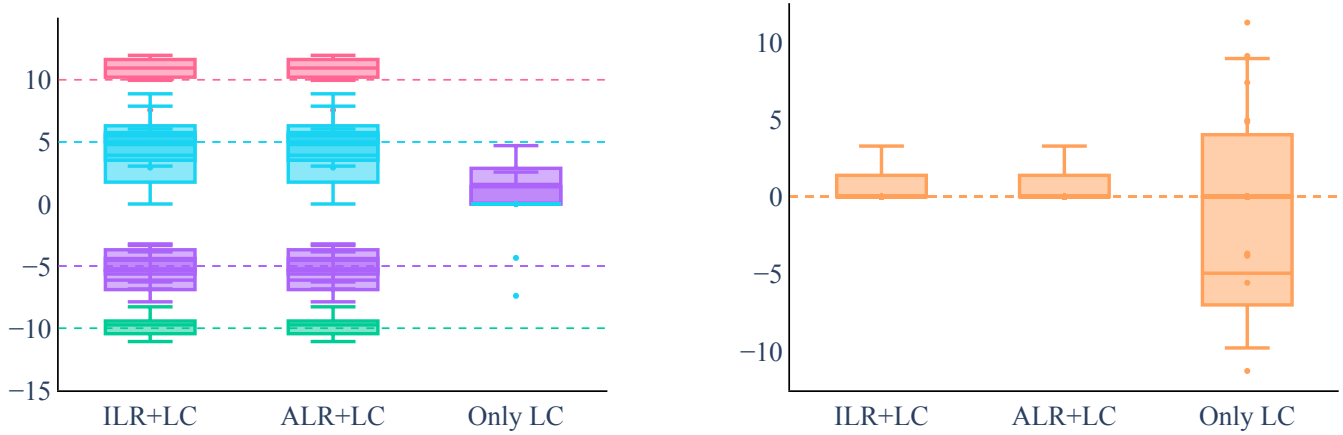


Figure S38. Setting B with $p = 250, q = 10$: The boxplots show the $\hat{\beta}$ values for the 20 runs for each of the 8 non-zero β coefficients (dashed lines, left) and the 242 zero β coefficients (dashed line, right). Only LC is not able to recover the β values at all. ILR+LC and ALR+LC are better suited to recover the causal parameters even when confounding is present. Despite the misspecified first stage, they are able to recover the causal β values on average.

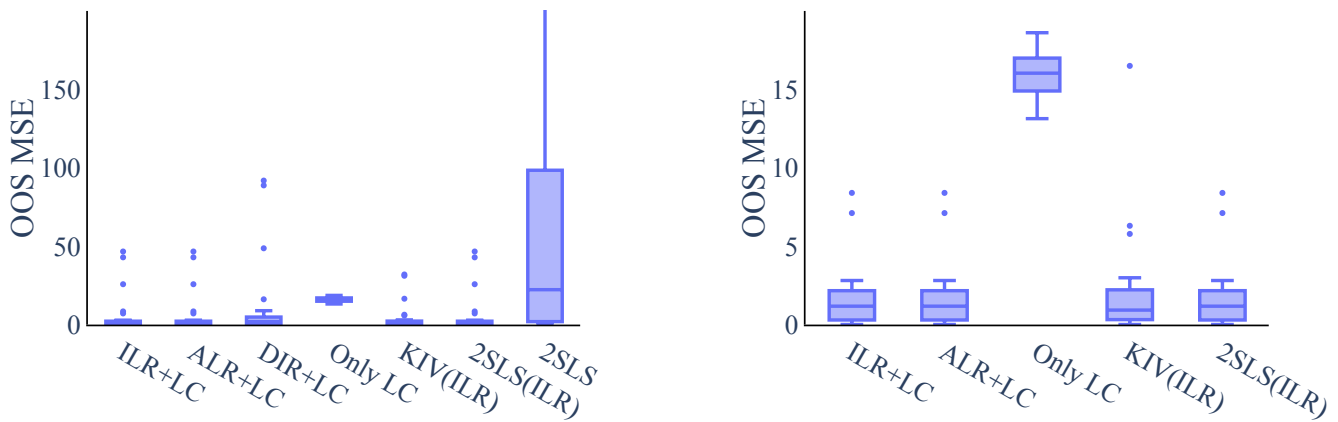


Figure S39. Setting A with $p = 3, q = 2$ and weak instruments: The boxplots show the OOS MSE of 50 runs. The DIR+LC performs considerably worse than all the other methods. The problem might stem from the “forbidden regression” issue coming from two misspecified stages. On the right hand side we adjusted the y-scale. The graph shows that the other wellspecified methods still outperform the naive regression in terms of OOS MSE in the weak instrument setting. We observe a higher variance in performance than in the stronger instrument setting.

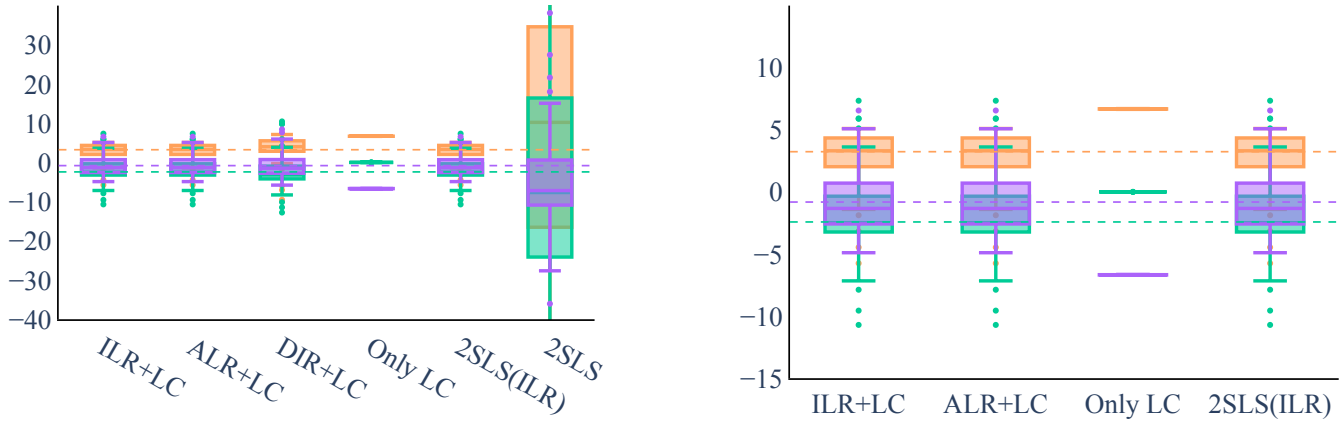


Figure S40. Setting A with $p = 3, q = 2$ and weak instruments: The boxplots show the $\hat{\beta}$ values for the 50 runs for each of the 3 β coefficients (dashed lines). In the weaker instrument setting, we are able to recover the true β values for the wellspecified two-stage methods, even though the variance of the $\hat{\beta}$ is higher while the naive regression is still subject to confounding (right, zoomed in plot). Only the DIR+LC is not able to recover the causal effect and seems biased toward the naive regression (left). This might be due to two misspecified stages.

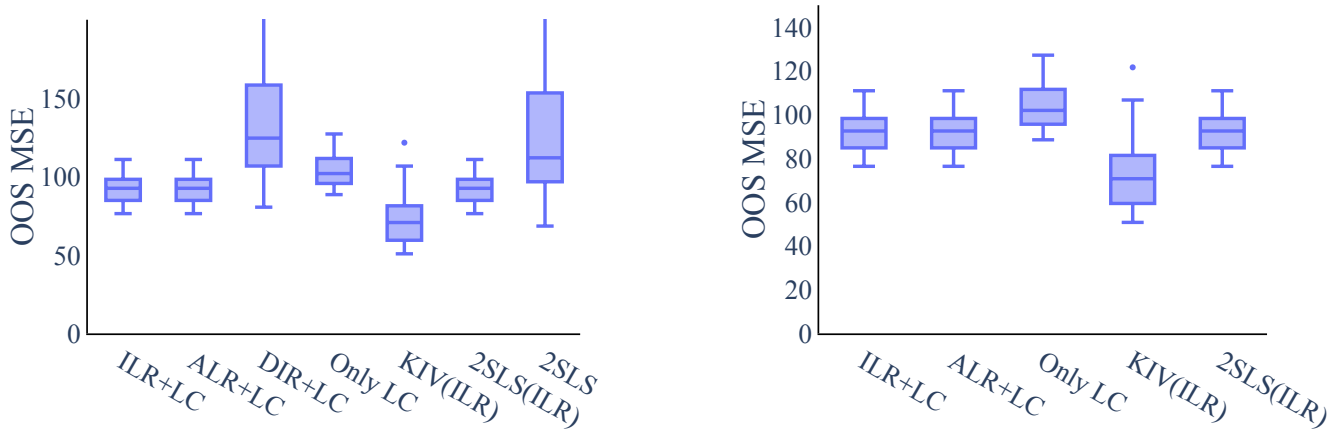


Figure S41. Setting A with $p = 3, q = 2$ and a non-linear function form of f : The boxplots show the OOS MSE of 50 runs. DIR+LC and 2SLS perform worst (left). The other two-stage approaches are able to recover the causal effect better than the naive regression. The correctly specified first stage helps in filtering out the confounding effect in the two-stage methods.

Non-linear Second Stage

Setting A with $p = 3, q = 2$ and a non-linear function form of f The two-stage methods perform well if they are in a wellspecified setting. With the DIR+LC method, however, it becomes obvious that misspecification can become problematic. Furthermore, wellspecification is typically impossible to ascertain in practice and most real-world examples are likely not perfectly linear. Thus, we add a polynomial X dependency term in the second stage to evaluate ALR+LC, ILR+LC and $2SLS_{ILR}$ on a partly misspecified setting.

Note that we can only look at the OOS MSE as the β values do not carry any causal interpretation (see Figure S41). The DIR+LC still suffers from two misspecified stages and performs worst. When only the second stage is misspecified, ALR+LC, ILR+LC and $2SLS_{ILR}$ still outperform the naive regressions. However, we are not able to capture the true causal effect because of the misspecification in the second stage. The overall error thus grows in all methods.

Scarce Data Example $p \gg n$

Setting A with $p = 250, q = 10$ and $n = 100$ Also for $n = 100$, the same problem of the lack of regularization persist. $2SLS_{ILR}$ and KIV_{ILR} do not perform well at all (Figure S42). For readability we thus omitted $2SLS_{ILR}$ from the β plots.

As against the large dataset example, the two-stage methods naturally show much larger confidence interval around their estimates, whereas the naive regression does not suffer at the same scale. However the naive regression has troubles to recover

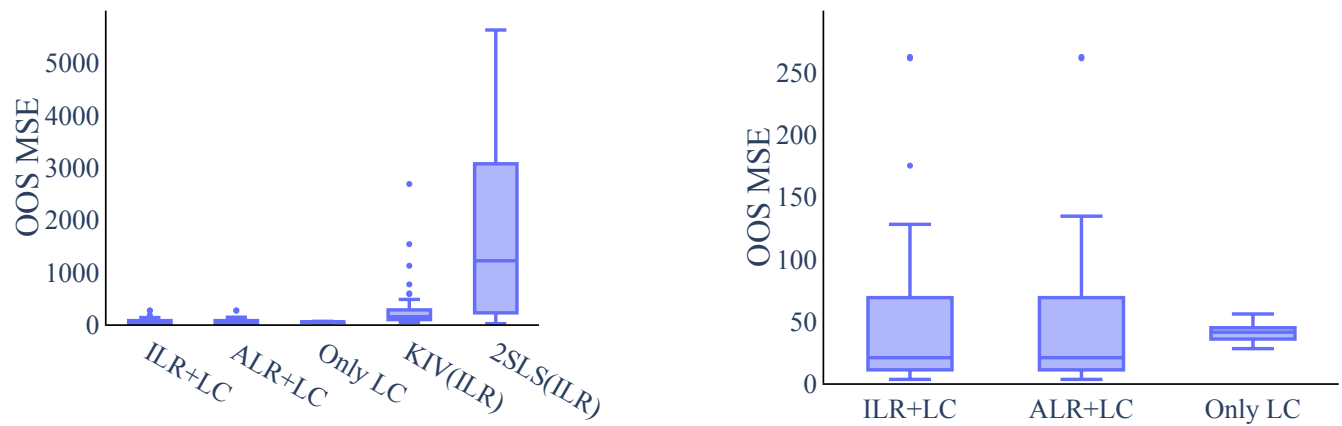


Figure S42. Setting A with $n = 100$, $p = 250$, $q = 10$: The boxplots show the OOS MSE of 50 runs. $2SLS_{ILR}$ and KIV_{ILR} are volatile and lack sensible regularization (left). This problem is more pressing as the dimensionality grows and the number of data samples decreases. When we adjust the y-scale, we see that also Only LC (right) performs worse compared to the regularized two-stage approaches. Note however, that the width of the confidence intervals of the two-stage approaches has increased compared to the larger dataset.

the full support (see Figure S43). Thus, even with a much larger uncertainty, the regularized two-stage approaches are able to recover the true causal β s.

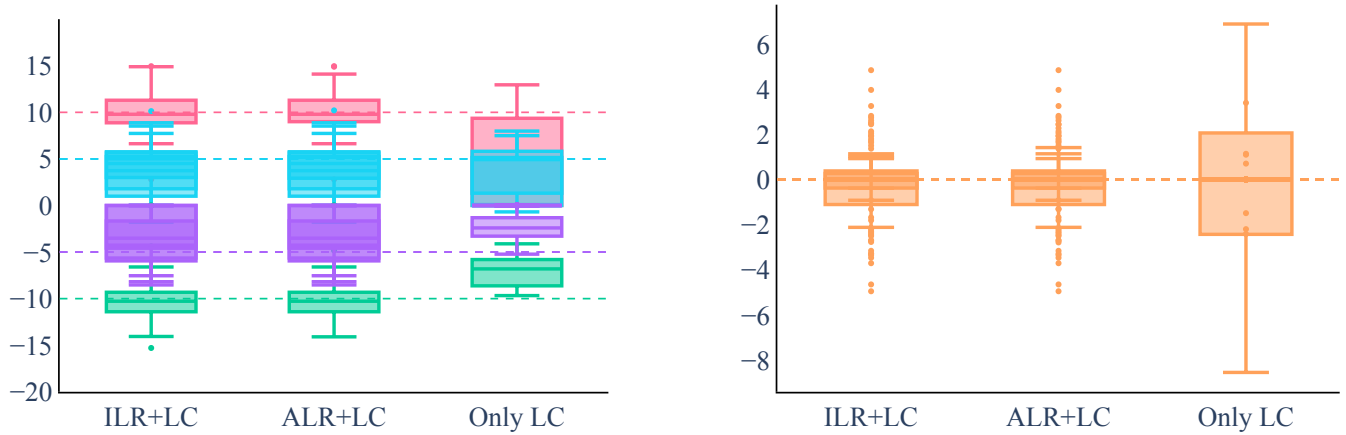


Figure S43. Setting A with $n = 100$, $p = 250$, $q = 10$: The boxplots show the $\hat{\beta}$ values for the 50 runs for each of the 8 non-zero β coefficients (dashed lines, left) and the 242 zero β coefficients (dashed line, right). The two-stage methods are able to recover the causal effect on average, whereas the naive regression method is not able to recover the true support. $2SLS_{ILR}$ does not produce sensible estimates due to the missing regularization and is omitted for better readability. Note however, that the width of the confidence intervals of the two-stage approaches has increased compared to the larger dataset.